

Global Relationships Among the Physical Properties of Stellar Systems

David Burstein

Department of Physics and Astronomy,
Box 871054, Arizona State University
Tempe, AZ 85287-1504

Ralf Bender

Universitäts-Sternwarte München
Scheinerstrasse 1
D-81679 München, Germany

S. M. Faber and R. Nolthenius

UCO/Lick Observatory
University of California
Santa Cruz, CA 95064 U.S.A.

ABSTRACT

The κ -space three-dimensional parameter system was originally defined to examine the physical properties of dynamically hot elliptical galaxies and bulges (DHGs). The axes of κ -space are proportional to the logarithm of galaxy mass, mass-to-light ratio, and a third quantity that is mainly surface brightness. In this paper we define self-consistent κ parameters for disk galaxies, galaxy groups and clusters, and globular clusters and use them to project an integrated view of the major classes of self-gravitating, equilibrium stellar systems in the universe. Each type of stellar system is found to populate its own fundamental plane in κ -space. At least six different planes are found: 1) the original fundamental plane for DHGs; 2) a nearly-parallel plane slightly offset for Sa-Sc spirals; 3) a plane with different tilt but similar zero point for Scd-Irr galaxies; 4) a plane parallel to the DHG plane but offset by a factor of 10 in mass-to-light ratio for rich galaxy clusters; 5) a plane for galaxy groups that bridges the gap between rich clusters and galaxies; and 6) a plane for Galactic globular clusters. We propose the term “cosmic metaplane” to describe this ensemble of interrelated and interconnected fundamental planes.

The projection κ_1 - κ_3 (M/L vs. M) views all planes essentially edge-on. Planes share the common characteristic that M/L is either constant or

increasing with mass. The $\kappa_1\text{--}\kappa_2$ projection views all of these planes close to face-on, while $\kappa_2\text{--}\kappa_3$ shows variable slopes for different groups owing to the slightly different tilts of the individual planes. The Tully-Fisher relation is the correct compromise projection to view the spiral-irregular planes nearly edge on, analogous to the $D_n\text{--}\sigma$ relation for DHGs. No stellar system yet violates the rule first found from the study of DHGs, namely, $\kappa_1 + \kappa_2 < \text{constant}$, here chosen to be 8. In physical terms, this says that the maximum global luminosity density of stellar systems varies as $M^{-4/3}$. Galaxies march away from this “zone of exclusion” (ZOE) in $\kappa_1\text{--}\kappa_2$ as a function of Hubble type: DHGs are closest, with Sm-Irr’s being furthest away.

The distribution of systems in κ -space is generally consistent with predictions of galaxy formation via hierarchical clustering and merging. The cosmic metaplane is simply the cosmic virial plane common to all self-gravitating stellar systems, tilted and displaced in mass-to-light ratio for various types of systems due to differences in stellar population and amount of baryonic dissipation. Hierarchical clustering from an $n = -1.8$ power-law density fluctuation spectrum (plus dissipation) comes close to reproducing the slope of the ZOE, and the progressive displacement of Hubble types from this line is consistent with the formation of early-type galaxies from higher $n\text{--}\sigma$ fluctuations than late Hubble types.

The M/L values for galaxy groups containing only a few, mostly spiral galaxies, vary the strongest with M . Moreover, it is these groups that bridge the gap between the two planes defined by the brightest galaxies and the lowest mass rich clusters, giving the cosmic metaplane its striking appearance. Why this is so is but one of four key questions raised by our study. The second question is why the slopes of *individual* Hubble types in the $\kappa_1\text{--}\kappa_2$ lie plane parallel the ZOE. At face value, this appears to suggest *less* dissipation of massive galaxies within their dark halos compared to lower-mass galaxies of the same Hubble type. The third is why we find isotropic stellar systems only within an effective mass range of $10^{9.5\text{--}11.75} M_\odot$. This would seem to imply that dissipation only results in galaxy components flattened by rotation in a limited mass range. The fourth question, perhaps the most basic of all, is how does M/L vary so smoothly with M among all stellar systems so as to give the individual tilts of the various fundamental planes, yet preserve the overall appearance of a metaplane? The answer to this last question must await a more thorough knowledge of how galaxies relate to many parameters, including: their environment, structure, angular momentum acquisition, density, dark matter concentration, the physics of star formation in general, and the formation of the

initial mass function in particular.

The present investigation is limited by existing data to the B passband and is strongly magnitude-limited, not volume-limited. Rare or hard-to-discover galaxy types, such as H II galaxies, starburst galaxies and low-surface-brightness galaxies, are missing or are under-represented, and use of the B band over-emphasizes stellar population differences. A volume-limited κ -space survey based on K-band photometry and complete to low surface brightness and faint magnitudes is highly desirable but requires data yet to be obtained.

Subject headings: galaxies — structure; galaxy clusters — structure

1. Introduction

It is now well established that orbital velocity increases strongly with galaxy luminosity in giant galaxies of all Hubble types. This relationship is embodied in the Tully–Fisher (Tully & Fisher 1977) relationship for spiral and irregular galaxies, and the fundamental plane (Dressler et al. 1987; Djorgovski & Davis 1987) for elliptical galaxies and spiral bulges (Dressler 1988; Bender, Burstein & Faber 1992; hereafter B²F1).

In B²F1 we developed a new way of viewing the structural properties of dynamically hot galaxies (hereafter DHGs) by making an orthogonal rotation of the global parameter space defined by velocity dispersion (σ), effective radius (r_e) and mean effective surface brightness within r_e (I_e). This rotation leads to a new coordinate system that we named “ κ -space” and which provides face-on and edge-on views of the DHG fundamental plane. The axes of κ -space are logarithmically related to galaxy mass, mass-to-light ratio, and a third quantity that depends primarily on surface brightness (the κ parameters are defined in § 2.2).

κ -space is a useful diagnostic tool for visualizing the physical properties of DHGs. It is therefore natural to ask whether an analogous plot for other Hubble types, and even galaxy groups and clusters, could be similarly informative.

Earlier discussions of the relationships among the physical properties of stellar systems concentrated on scaling relationships between just two parameters at a time. Examples are the Tully–Fisher (TF) relation for spirals and the Faber–Jackson (1976) relation for ellipticals: $L \propto V^4$. We now understand that, for elliptical galaxies, $L \propto V^4$ is just one projection of what is inherently a two-dimensional family, the fundamental plane (FP). It is natural to conjecture that the TF relation is a similar projection for spiral and

irregular galaxies, but this has not yet been shown explicitly. If there is a FP for spirals and irregulars, what is its relation to the DHG FP, and how do the various Hubble types distribute themselves within it?

The various scaling relations for stellar systems provide a test for theories of structure formation in the the universe. Faber (1982a,b) and Blumenthal et al. (1984; hereafter BFPR), among others, examined the projected distributions of galaxies and clusters onto the (density, velocity) and (mass,velocity) planes and compared them to the predictions of hierarchical clustering theory. The distributions of rich galaxy clusters (Schaeffer et al. 1993) and globular clusters (Djorgovski 1995) were examined in standard FP space. These latter were found to form planes nearly parallel to the DHG FP.

Despite these individual investigations, there still has not been a unified survey of all types of self-gravitating, equilibrium stellar systems in the three-dimensional space of their fundamental structural parameters. In this paper we assemble the necessary database to provide such a survey. A preliminary version of this work was presented in Burstein et al. (1995; hereafter B²FN). Here we describe how our homogeneous and self-consistent data set has been assembled and how the structures of the major groups of self-gravitating stellar systems fit together in κ -space. We discuss how their overall distribution can be interpreted in terms of hierarchical clustering theory. A parallel goal of this effort is to make available a benchmark data set against which the success of models for structure formation in the universe can be judged. Finally, our catalog of local structural parameters is a foil for similar structures at high redshift, for the purpose of detecting and quantifying the evolution of structure in the universe using the lookback effect.

The database contains the most familiar self-gravitating, virialized or nearly-virialized systems in the nearby universe, including galaxies, globular clusters, groups of galaxies, and large clusters of galaxies. However, rare types of galaxies are missing or underrepresented, e.g. starburst H II galaxies (e.g., Salzer et al. 1989; Gallego et al. 1996), compact, narrow emission line galaxies (Koo et al. 1994) and very low surface brightness galaxies (e.g., McGaugh 1996; Dalcanton 1997). Thus, the true volume populated by galaxies in κ -space is likely to be more extended to both lower and higher surface brightnesses than shown here. Our galaxy sample is also approximately magnitude-limited, so that the number density versus position in κ -space is not an accurate picture of the local volume densities of galaxies. Even with these shortcomings, the present data are a useful first overview of the properties of common structures in the nearby universe.

Definitions of κ -space parameters are reviewed in § 2 and explicitly equated to typical galaxy parameters such as mass, radius and luminosity in Appendix A. In § 3 we develop a more appropriate way (than used in B²FN) to intercompare the properties of galaxies of

different morphological types, as well as to homogenize the properties of galaxy groups, galaxy clusters and globular clusters. § 4 is a picture gallery that shows, in various projections, how different types of galaxies are distributed within κ -space. The κ -space distributions of galaxy groups, galaxy clusters and globular clusters are compared to those of galaxies in § 5, and tested with N-body models in Appendix B. In § 6 we discuss how these data accord with the current picture of hierarchical structure formation in the universe. Our results are summarized in § 7.

2. Data

2.1. Data Needed for κ Parameters

Following B²F1, we choose to define the photometric parameters of stellar systems using the B passband. This choice is dictated by the large database of available B photometry. It would clearly be valuable to see how these properties relate in another passband, particularly one less sensitive to stellar population age such as near-infrared K. Unfortunately, the data do not yet exist to do so, nor are they likely to appear soon in the quantity currently available for B-band data.

The global structure of self-gravitating, equilibrium stellar systems can be characterized by three parameters: size, surface brightness, and internal orbital velocity. We use the photometric data to measure the radius containing half the luminosity (the effective radius, r_e) and the mean surface brightness within this effective radius (I_e). As a measure of orbital velocity we use the *one-dimensional central* velocity dispersion (σ_c). This is arbitrary, as arguments could be made to use the mean velocity dispersion within the effective radius for galaxy clusters, say, or mean rotation speed for spiral and irregular galaxies. Our choice of central velocity dispersion follows the convention of B²F1, but we will need to generate this parameter from other types of orbital velocity measurements (see below). This section presents the basic sources of initial data. In § 3 we discuss how the data are placed onto a common system.

2.2. Definition of κ -Parameters

The κ -space parameters are defined as follows:

$$\kappa_1 \equiv (\log \sigma_c^2 + \log r_e) / \sqrt{2}, \quad (1)$$

$$\kappa_2 \equiv (\log \sigma_c^2 + 2 \log I_e - \log r_e) / \sqrt{6} \quad (2)$$

and

$$\kappa_3 \equiv (\log \sigma_c^2 - \log I_e - \log r_e) / \sqrt{3}. \quad (3)$$

The quantity σ_c is the central velocity dispersion in km s^{-1} . As in B²F1, r_e is measured in kpc, while I_e is measured in units of B-band solar luminosities pc^{-2} , computed as $10^{-0.4(SB_e - 27.0)}$ where SB_e is the mean B-band surface brightness in B mag arcsec⁻² within r_e .

In many cases it useful to have convenient transformations between the κ parameters and such typical parameters for stellar systems such as mass, luminosity, size, mass-to-light ratio, etc. In the present paper we use such transformations in many ways, in order to interpret the properties of stellar systems. As such, in Appendix A we give the equations that transform the κ parameters to these common parameters, including all the other parameters we employ in this paper.

2.3. Distances

Distances for galaxies, galaxy groups and galaxy clusters are determined using Local Group radial velocities and an assumed smooth Hubble flow with $H_0 = 50 \text{ km sec}^{-1} \text{ Mpc}^{-1}$ (cf. B²F1). In adopting this prescription we are purposefully ignoring real peculiar motions, as these motions would currently have to be derived from the very physical properties of the stellar systems we wish to study. This approach is adequate as our goal is to discuss the physical relationships among stellar systems in broad-brush strokes. Distances for ellipticals, bulges and dwarf ellipticals are based on their group or individual radial velocities as tabulated by Faber et al. (1989) and B²F1. Most spiral and irregular galaxy distances are based on individual Local Group radial velocities as given in de Vaucouleurs et al. (1991, hereafter RC3).

There are three exceptions to the use of a smooth Hubble flow and Local Group radial velocities. Fifteen spirals and all DHGs whose radial velocities and structural properties place them in the virialized parts of Virgo or Coma are given the distances of their respective clusters. The Virgo cluster distance is assumed to be 20.7 Mpc (based on an assumed Local Group velocity for the cluster of 1035 km sec^{-1}). The Coma cluster distance is as in B²F1, 137.9 Mpc, based on a Local Group velocity of $6,895 \text{ km sec}^{-1}$. Local Group

DHGs are given distances as in B²F1. Local Group spiral and irregular galaxies are put either at the generally-accepted distance of M31 (0.7 Mpc) or of M33 (1 Mpc). Globular cluster distances in our Galaxy are determined from the V mag of the horizontal branch, as listed by Peterson (1993).

2.4. Dynamically Hot Galaxies

The κ parameters for DHGs with measures of internal orbital anisotropy are given in B²F1. The reader is referred to that paper for details. The present catalog contains 292 additional elliptical galaxies from Faber et al. (1989) lacking anisotropy measures and not included in B²F1.

2.5. Spiral and Irregular Galaxies

Observed κ parameters for spiral and irregular galaxies are derived from data in the RC3. A search was made of the computer-readable copy of the RC3 (kindly supplied by H.G. Corwin, Jr.) for galaxies with listed values of radial velocity, B-band values of SB_e , angular radius θ_e and observed velocity widths ΔV (W_{20} in RC3 terminology). We accept the RC3 definitions of ΔV , inclination and effective radius and define rotation velocity as $V_{rot} = \Delta V/2 \sin i$ (where $\sin i = \arccos[\sqrt{(b/a)^2 - 0.04}/0.96]$ and a/b is the axial ratio taken from the RC3). Known errors in determining V_{rot} are at the 10% level (RC3), comparable to the errors of velocity dispersions (Davies et al. 1987).

From this first cut, we exclude all galaxies labeled as “peculiar,” those with inclinations more face-on than 45°, and those with Galactic extinction $A_B > 0.75$ mag, as predicted by the method of Burstein & Heiles (1978, 1982). We also exclude three Sa galaxies (UGC 1344, NGC 4424 and NGC 7232) for which the tabulated values of V_{rot} are apparently in error (too low). This leaves 511 galaxies of Hubble types Sa through Im.

To derive mean effective surface brightness and radius we have corrected the RC3 values of circular effective aperture size (A_e) and mean surface brightness within A_e (termed m'_e in the RC3) using the axial-ratio-based statistical relationships defined in the RC3. In addition, the surface brightnesses of all spiral galaxies have been corrected for Galactic extinction and for internal extinction by subtracting $1.5 \log(a/b)$ mag. This is an average correction taken from the RC3 analysis. The inclination-based corrections to translate A_e and m'_e to r_e and I_e are typically small (0.04 dex and 0.08 dex respectively for $\log(a/b) = 0.4$). Internal extinction corrections are larger (± 0.3 mag) for a range of inclinations

corresponding to $\log(a/b) = 0.4$ to 0.8 . The internal corrections for extinction correct the galaxy to face-on.

The effective photometric parameters for spiral galaxies from the RC3 are affected by errors in axial ratio, A_e and m_e' , which combine to produce errors of order >0.1 dex in r_e and SB_e . Since such errors dwarf either K-corrections (<0.04 dex) or cosmological corrections, (<0.03 dex to SB_e), we choose not to make these further corrections for the spiral galaxy data. As we will see, errors of 0.1 dex have no effect on our conclusions.

In addition to the RC3 data, κ parameters are derived for two large, low surface brightness spiral galaxies identified by Impey & Bothun (1989; Malin 1) and by Bothun et al. (1990; which we call here Malin 2). Rotation velocity, effective radii and effective surface brightnesses are derived from data in these papers, with distances adjusted to our assumed value of $H_0 = 50 \text{ km sec}^{-1} \text{ Mpc}^{-1}$. Values of r_e and SB_e for these two galaxies are probably no more accurate than 0.15 dex, and the value for rotation velocity no better than 15% . As above, these uncertainties have no effect on our conclusions.

2.6. Galaxy Groups

The only genuinely new data in this paper are structural parameters for galaxy groups (as opposed to clusters, see below). Appendix B shows selecting groups in real-space vs. redshift space changes group parameters by a systematic but very small amount, compared to the overall spread in physical properties among groups, and does not affect our conclusions.

The galaxy groups here come from the *Nearby Groups Catalog* of Nolthenius (1993; hereafter N93). The N93 groups were identified from the $m_{lim} = 14.5$ CfA1 catalog of Davis et al. (1982), and those used here have at least 3 members. Following Geller & Huchra (1983) and Nolthenius & White (1987), the N93 groups are identified by a percolation algorithm linking galaxies on the sky and in redshift so that the number overdensity threshold should be constant with redshift. In N93 the sky separation linking criterion (D_0) is chosen to be less than 0.36 of the mean intergalaxy separation, which corresponds to a limiting number overdensity of ≥ 20 . The redshift link scales with depth according to sample completeness and is 350 km sec^{-1} at a distance of 5000 km sec^{-1} (corresponding to a redshift link parameter $V_5 = 350$; see N93).

For computing group surface brightnesses and M/L , we have used fully-corrected $B_T(0)$ magnitudes for the individual galaxies on the RC3 system. These are available for 96% of the galaxies. This ensures that the photometric κ parameters for the individual

galaxies and groups are on the same system. Only 45 of the 1095 galaxies in 170 groups (excluding the Abell 194 and Coma clusters, which are also in the Schaeffer et al. (1993) cluster sample) do *not* have quoted RC3 values of $B_T(0)$. For these 45 galaxies alone we use the B_T values given by N93.

The half light radius r_e for a group is found by taking a luminosity-weighted centroid of the visible galaxies, and the radius enclosing half the visible light is interpolated. We considered unweighted centroids and found that the extent and tightness of groups in κ -space was virtually identical. We prefer L -weighted centroids as these more closely parallel the method used to define the photocenters of galaxies. To be further consistent with the parameters for galaxies, other sources of baryonic flux (e.g., X-ray emitting hot gas) are not considered. The values of r_e and SB_e for galaxy groups are probably accurate at the 0.3 dex level.

Velocity dispersions for the n -visible galaxies in a group with redshifts v_i are found from

$$\sigma^2 = \frac{1}{(n-1)} \sum_i^n (v_i - \bar{v})^2. \quad (4)$$

Velocity dispersions determined in this manner refer essentially to the effective radius of the group, σ_e . In contrast, the velocity dispersions for DHGs are measured at their centers, σ_c . We take account of this difference in § 3.2.

In addition to the observed κ parameters and related data for groups, we also calculate the fraction of E+S0 galaxies. This fraction can be taken as the analog of Hubble type for individual galaxies. An E/S0 fraction of 1/3 is taken as the dividing line between E-rich ($> 1/3$ E/S0's) and E-poor ($\leq 1/3$ E/S0's) groups.

2.7. Galaxy Clusters

Schaeffer et al. (1993) have shown that the physical properties of 16 rich clusters of galaxies define a fundamental plane similar in slope but offset in zero point from that defined by elliptical galaxies. A. Cappi kindly supplied us with a computer-readable list of the data used by Schaeffer et al. These velocity dispersions refer approximately to r_e , so we correct them to σ_c as for groups (see § 3.2). κ parameters are calculated after revising the Schaeffer et al. distance scale to $H_0 = 50$. Since the Schaeffer et al. clusters are among the richest nearby large clusters, we assume that all are E-rich by our group-based criterion.

2.8. Globular Clusters

κ parameters for 51 globular clusters are based on tables given in the appendices to “Structure and Dynamics of Globular Clusters” (Djorgovski & Meylan 1993). Half light radii are taken from Trager, Djorgovski & King (1993), σ_e from Pryor & Meylan (1993), and distances, $E(B - V)$, total V magnitude, and $B - V$ colors from Peterson (1993). The effective radius is the half light radius given by Trager et al., and the effective V magnitude is 0.75 mag ($\times 2$) fainter than the total V magnitude listed by Peterson. B-band surface brightness (to derive I_e) is obtained by correcting both $B - V$ and V for reddening and extinction using $A_V = 3E(B - V)$. Most of the globular clusters have reliable measurements of half light radii and total V mag; for several, one of these quantities is more uncertain than the other. Clusters are excluded that have poor observational data for both quantities, as these are seen to scatter more within κ -space.

3. Homogeneous κ -space Parameters for Different Stellar Systems

3.1. Effective Radius and Effective Surface Brightness

The definition of r_e as the radius encompassing half the light is standard for all galaxy types and globular clusters and is straightforwardly extended to galaxy groups and clusters (see above). Ideally, we would wish that our values of r_e and I_e referred to the *total* baryonic mass distribution, not just that of the stars, but by using B-band light we are ignoring all non-stellar baryons. For dwarf irregular galaxies, B-band r_e values are likely to underestimate the baryonic half-mass radius since many such galaxies have extended H I gas distributions (e.g. DDO 154, Krumm & Burstein 1984). I_e likewise underestimates the baryonic surface density by ignoring H I and H₂. Values of r_e and I_e for groups and clusters ignore the distribution of hot X-ray emitting gas known to be a major baryonic component of clusters (e.g., Fabian 1994) and more recently found in smaller E-rich galaxy groups (e.g., Mulchaey et al. 1996). As the X-ray gas appears to be more extended than the galaxies (Mulchaey et al. 1996), this could lead to underestimation of baryonic values of r_e for these stellar systems by 20–50%, and underestimation of baryonic surface density by up to a factor of 3.

Even for stars, the B band is susceptible to perturbing effects. B-band parameters are reasonably consistent for DHGs, globular clusters, and E-dominated groups and clusters, but the light of spiral and irregular galaxies (and spiral-dominated groups/clusters) is strongly perturbed by dust and young stars. While we might attempt to correct I_e between spirals and DHGs for stellar population-related mass-to-light differences, we choose not to

do so for two reasons. First, the range of stellar populations among spirals of similar Hubble type is nearly as large as that between spiral galaxies and elliptical galaxies (Burstein 1982). Second, models of stellar populations (Worthey 1994) indicate that such corrections typically change M/L in the B passband by $\sim \times 2$, leading to κ_3 errors of less than 0.3 dex.

The presence of the above systematic trends and omissions is clearly evident in the data, most obviously in values of M/L for different types of objects. However, present knowledge does not permit us to account for these effects in any reliable way. To compile the survey, we prefer to stay firmly rooted in a well defined and internally consistent database (B-band photometry) and leave such corrections to the future.

3.2. Characteristic Internal Velocity

The most difficult parameter to define homogeneously for different types of stellar systems is characteristic internal velocity. In keeping with our philosophy, we would like to define a velocity that is simply related to a system’s mass. This σ_{ideal} would combine with r_e to yield a mass that is consistently measured for all stellar systems. How to define such a σ_{ideal} is not clear, but we can operationally define transformations among common velocity systems to bring them reasonably close onto the same system.

.For the present sample, there are three kinds of characteristic velocities: i) σ_c , the central velocity dispersion, used for giant E galaxies and the bulges of spiral galaxies (B²F1); ii) σ_e , the velocity dispersion near within r_e , used for globular clusters, galaxy groups and galaxy clusters; and iii) V_{rot} , the maximum circular rotation velocity for disk galaxies. σ_c and σ_e are line-of-sight, 1-D measures of dispersion, which is correlated with the local profile slope as well as mass, whereas V_{rot} relates mainly to enclosed mass alone. The goal is to identify relationships among these three parameters that will, on average, permit us to transform one measurement into another to an accuracy of ~ 0.1 dex. Two such transformations are needed: $\log \sigma_c = \log \sigma_e + K_1$ and $\log \sigma_c = \log V_{rot} + K_2$, where the task is to estimate the values of K_1 and K_2 .

The relationship between σ_e and σ_c is known for King (1966) and Jaffe (1983) models (Appendix A of B²F1; Chapter 4 in Binney & Tremaine 1987). A reasonable compromise ($\pm 10\%$) is $\sigma_e/\sigma_c = 0.84$, yielding $K_1 = +0.076$ dex. We assume that globular clusters and galaxy groups and clusters obey King-Jaffe models. The additive corrections to be applied to the κ parameters from this correction are small: $\Delta_1(\kappa_1) = 0.11$ dex, $\Delta_1(\kappa_2) = 0.06$ dex, and $\Delta_1(\kappa_3) = 0.09$ dex.

Should we also consider making a correction for anisotropy in the velocity dispersion?

Before doing so, one should recognize that there are really two kinds of anisotropy. One is x - y - z anisotropy, which leads to a range of flattenings and triaxialities as, for example, in luminous E galaxies (B²F1). The other is determined by the ratio of radial-to-tangential orbital motions. These two anisotropies can coexist in the same object. Fortunately, it seems that x - y - z anisotropy is benign in κ -space, as shown by the fact that apparent galaxy ellipticity plays a negligible role in the scatter of DHGs relative to the fundamental plane (cf. Saglia, Bender & Dressler 1992; Jørgensen, Franx & Kjaergaard 1996). Little information is available on radial-to-tangential anisotropy, but hot systems that formed via violent relaxation should not be strongly radially anisotropic at the 10% level of accuracy needed here. Hence we make no corrections for either type of anisotropy to the velocity dispersions of DHGs.

For spiral and irregular galaxies with exponential Freeman (1970) disks and central surface brightnesses equal to 21.65 B mag arcsec⁻², the effective radius occurs at 23.47 B mag arcsec⁻². Among galaxies with central surface brightnesses within 1 mag arcsec⁻² of this value, most objects have reached their observed maximum rotation velocity by r_e or are close to it (Rubin et al. 1985), so it is reasonable to assume that V_{rot} is measured at r_e . For disks embedded in isotropic isothermal halos, we expect $V_{rot}/\sigma_c = \sqrt{2}$ (Binney & Tremaine, 1987, Eq. 4–55), which agrees with observed values (Whitmore & Kirshner 1981). We therefore set $K_2 = -0.151$ dex and find $\Delta_2(\kappa_1) = -0.21$ dex, $\Delta_2(\kappa_2) = -0.12$ dex, and $\Delta_2(\kappa_3) = -0.17$ dex. These corrections are again small compared to the range of κ parameters for stellar systems.

The zero point corrections to the κ parameters are summarized in Equations 5 to 10. For spiral and irregular galaxies, the κ -parameters are:

$$\kappa_1 = (\log V_{rot}^2 + \log r_e)/\sqrt{2} - 0.21, \quad (5)$$

$$\kappa_2 = (\log V_{rot}^2 + 2\log I_e - \log r_e)/\sqrt{6} - 0.12, \quad (6)$$

and

$$\kappa_3 = (\log V_{rot}^2 - \log I_e - \log r_e)/\sqrt{3} - 0.17. \quad (7)$$

For all other stellar systems (except DHGs), which require conversion of σ_e to σ_c , the equations become:

$$\kappa_1 = (\log \sigma_e^2 + \log r_e)/\sqrt{2} + 0.11, \quad (8)$$

$$\kappa_2 = (\log \sigma_e^2 + 2 \log I_e - \log r_e) / \sqrt{6} + 0.06, \quad (9)$$

and

$$\kappa_3 = (\log \sigma_e^2 - \log I_e - \log r_e) / \sqrt{3} + 0.09. \quad (10)$$

3.3. The Listing of the Data

Table 1 lists the data for our sample (the first page only is printed for the journal). The full table is electronically available in a convenient ASCII format through this journal, the Astrophysical Data Center (ADC), and via anonymous ftp from samuri.la.asu.edu (129.219.144.156; cd to pub/kappaspace)

Column 1 gives the common name for the object (N = NGC; U = UGC; E = ESO number; M = MCG number; ZW = Zwicky catalog number; ABELL for Abell Cluster; GP for Nolthenius group number). Column 2 gives an internal identifying number. In Column 3 we give a numerical code for the type of object (the following number in parentheses are the number of objects of each type in the catalog): 1 for anisotropic gE or cE galaxies (41); 2 for isotropic gE, cE galaxies or bulges of S0s (51); 3 for isotropic dE galaxies (3); 4 for anisotropic dE galaxies (8); 5 for 7 Samurai elliptical galaxies with no isotropy measure (292); 7 for dSph galaxies with no isotropy measure (5); 10 for Sa galaxies (62); 11 for Sab–Sb galaxies (106); 12 for Sbc galaxies (89); 13 for Sc galaxies (129); 14 for Scd–Sdm galaxies (47); 15 for Sm galaxies (33); 16 for Irr galaxies (45); 18 for the galaxies Malin 1 and Malin 2 (2); 20 for spiral-rich galaxy groups with only 3 galaxies (56); 21 for spiral-rich galaxy groups with 4 galaxies (17); 22 for spiral-rich galaxy groups with between 5 and 8 members (32); 23 for spiral-rich galaxy groups with between 9 and 18 members (9); 24 for spiral-rich galaxy groups of 19 members or more (4); 30 for E-rich groups with 3 galaxies only (12); 31 for E-rich groups with 4 galaxies (20); 32 for E-rich groups with between 5 and 8 galaxies (14); 33 for E-rich groups with between 9 and 18 galaxies (3); 34 for E-rich groups with between 19 and 113 galaxies (3); 35 for the 16 rich clusters sampled by Schaeffer et al. (1993) (16); and 40 for the globular clusters (51).

Column 4 gives the distance in units of Mpc ($H_0 = 50 \text{ km sec}^{-1} \text{ Mpc}^{-1}$). Column 5 gives the log of the original characteristic internal velocity (σ_c for gE, cE, Bulges and 7 Samurai ellipticals; V_{rot} for spirals and irregulars ($\log V_{char, obs}$); σ_e for everything else). Column 6 gives either the observed value of $\log \sigma_c$ or the transformed value as discussed in § 3.2 ($\log \sigma_{c, used}$). Columns 7 and 8 give, respectively, the values of $\log r_e$ in kpc and

$\log I_e$ in $L_\odot \text{ pc}^{-2}$ used to calculate the κ parameters. These B-band photometric parameters are corrected for Galactic extinction and internal extinction, usually by the original source of data (§ 3.1). No K-corrections or cosmological corrections have been applied.

Column 9 gives either the reddening-corrected and K-corrected $B - V$ color or, in the case of galaxy groups and galaxy clusters, the fraction of E+S0 giant galaxies. Columns 10, 11 and 12 give the κ parameters. Columns 13 and 14 give the quantities $\delta_{2:1}$ and $\delta_{3:1}$ defined in § 4.7. Columns 15, 16 and 17 give effective mass, $\log M_e$, effective B-band luminosity, $\log L_e$ and effective B-band mass-to-light ratio, $\log(M_e/L_e)$ in solar units. Column 18 gives the equivalent virial temperature of the object within the effective radius, $\log T_e$. Lastly, Column 19 gives the estimated baryon number density $\log n_{\text{bary},e}$ (cm^{-3}). The equations to generate many of the more familiar quantities derived from the κ parameters are given in Appendix A.

4. Galaxies in κ -Space

4.1. Spiral and Elliptical Galaxies in the Virgo and Coma Clusters

Figure 1 shows the distribution in κ -space for 48 gE in the Virgo and Coma clusters (cf. Figure 1 of B²F1) plus 15 spiral galaxies, Hubble types Sa through Sc/d, in Virgo. (These graphs differ slightly from those shown in B²FN owing to the K_1 velocity corrections made to the spiral galaxy κ parameters here.) We have previously shown that, when distances are defined as they are here, the Virgo and Coma gE samples define a very thin fundamental plane. Figure 1 is a two-dimensional fold-out of three-dimensional κ -space. By viewing the points projected onto all three planes, one can reconstruct their distribution in three dimensions. Two particular features of these diagrams are highlighted.

The FP defined by gEs in Virgo and Coma is given by the dark solid line in κ_1 - κ_3 (where the FP is viewed edge-on by design). Its equation is:

$$\kappa_3 = 0.15\kappa_1 + 0.36, \tag{11}$$

or, in solar units

$$\log(M_e/L_e) = 0.184 \log M_e - 1.25. \tag{12}$$

Equation 12 is the conventional definition for the DHG FP in terms of mass-to-light ratio: $M_e/L_e \propto M_e^{0.184}$. The FP projects onto κ_2 - κ_3 as a thick band, the midsection of which is

represented by the light solid line in this projection, the dotted lines indicating the upper and lower boundaries of the DHGs. The FP projects nearly face-on in $\kappa_1\text{--}\kappa_2$, where the distributions of DHGs and spirals are both very broad. The short dark lines drawn in each panel of Figure 1 and subsequent figures represent the effect of distance errors of $\pm 30\%$. Distance errors owing to real peculiar motions of galaxies up to this amplitude are the dominant source of observational scatter in all diagrams save Figure 1.

As is evident, the physical properties of the spiral galaxies in Virgo occupy a similar distribution in κ -space to the elliptical galaxies. There is much overlap in $\kappa_1\text{--}\kappa_2$, with offset but parallel distributions in the other two projections. The Virgo spirals thus define a second fundamental plane that is nearly parallel to the DHG FP but shifted to lower mass-to-light ratios by about a factor of two at fixed mass.

4.2. The Zone of Exclusion (ZOE) in $\kappa_1\text{--}\kappa_2$

The diagonal dotted line in the $\kappa_1\text{--}\kappa_2$ plane in Figure 1 delineates the empirically-determined “zone of exclusion” (hereafter called ZOE) for DHG galaxies (B²F1). Its equation is

$$\kappa_1 + \kappa_2 \leq 8 \tag{13}$$

The zero point here is adjusted slightly from the value 7.8 used in B²F1 to make the exclusion line exclude essentially all stellar systems including rich clusters (see below). Note that the Virgo spirals obey the same ZOE as the DHGs. This is a theme we will return to later: the ZOE is *universal* for the present sample of galaxies and clusters.

We define an effective volume density $j_e \equiv L_e \times (4/3\pi r_e^3)^{-1}$, which in the current system of units is $0.75 \times 10^{-3} I_e / r_e L_\odot \text{ pc}^{-3}$. Equation 13 can then be recast as

$$\log M_e + 0.73 \log j_e \leq 10.56, \tag{14}$$

or approximately

$$j_e \leq \text{const.} \times M_e^{-4/3}. \tag{15}$$

In other words, the maximum allowed luminosity volume density for collapsed stellar systems scales as $M_e^{-4/3}$. The significance of this condition will be made clear when we

examine the distribution of all stellar systems relative to the ZOE.

4.3. Dynamically Hot Galaxies

Figure 2 plots the distribution of all DHGs in κ -space. This distribution has been extensively discussed elsewhere (B²F1; Bender, Burstein, & Faber 1993a,b, 1995). In the present figures we divide the DHGs into six subsets for plotting purposes: isotropic and anisotropic giant Es, compact Es and bulges; isotropic and anisotropic dwarf ellipticals; giant Es from Faber et al. (1989) and dwarf spheroidals. These categories are defined and explained in B²F1.

DHGs divide into two major families that are most clearly seen in κ_1 – κ_2 : giant galaxies (upper right), which we call the Gas-Stellar Continuum in B²F1, and dwarf galaxies (lower left). This is analogous to the division of DHG systems into giants and dwarfs found by Kormendy (1988). Within the Gas-Stellar Continuum, more massive giant galaxies tend to have lower surface brightness (lower κ_2), while more massive dwarf galaxies tend to have higher surface brightness. Thus, in κ_1 – κ_2 the two families are at approximately right angles to one another (Figure 2).

In B²F1, we proposed the name Gas-Stellar Continuum because several properties vary along the giant sequence in a way that suggests that a varying fraction of gas (vs. stars) was involved in the last major merger. For example, giant ellipticals rotate slowly, are typically anisotropic in their velocity distributions, and tend to have boxy isophotes. Less massive ellipticals tend to be isotropic in velocity dispersion, rotate rapidly and have disk isophotes (Davies et al. 1983; Bender 1988; Kormendy & Bender 1996). Bulges continue the trend from less massive ellipticals. As discussed in B²F1 (see also references cited therein), these data suggest a merger formation picture in which the latest mergers that formed the smaller galaxies contained considerable gas, whereas those that formed the more massive ones had progressively more stars. Recently measured central density profiles (Faber et al. 1997) are consistent with this view. For brevity, in what follows we will refer to the giant DHG galaxies that comprise the Gas-Stellar Continuum as “giant ellipticals,” or gEs, despite the fact that this sequence also contains compact Es and bulges.

The dwarf family of DHGs is offset from the giant family to higher M/L in κ_1 – κ_3 , and this trend becomes extreme among the dSph, which are heavily dominated by DM. It is likely that they have lost baryons by galactic winds (Dekel & Silk 1986), ram-pressure stripping (Lin & Faber 1983), or some other means. B²F1 discussed ways in which the dwarf E family might evolve to or from the giants, but options are limited. Present-day

dwarf Es cannot be merged to produce present-day gEs as their stellar populations are too different (B²F2). Conversely, if dE and dSph are formed from other Hubble objects via either galactic winds or ram-pressure stripping, B²F1 showed that their progenitors are not visible among the other DHGs. However, they do seem to be compatible with baryon mass loss from late-type spiral and/or Irr progenitors, as discussed below.

4.4. Spiral Galaxies of Types Sa, Sab and Sb

Figure 3 shows the distribution within κ -space for spiral galaxies of Hubble types Sa to Sb (RC3 type numbers 1 to 3). This figure illustrates several points:

1) Early-type spiral galaxies are distributed similarly to gEs but offset slightly in each κ -space projection. Sa–Sb galaxies lie farther from the ZOE than gEs.

2) Sa–Sb galaxies define their own FP relation in κ_1 – κ_3 that is nearly parallel to that of gEs but slightly offset to lower values of M/L by about 0.3 dex. This is consistent with the Virgo cluster spirals (Figure 1).

3) There is a slight tilt to this plane in κ_2 – κ_3 compared to the nearly level distribution of DHGs in Figure 2. While barely visible here, this tilt becomes progressively more pronounced for later Hubble types. We will find in § 4.8 that it is the key that yields the TF relation.

4.5. Spiral Galaxies of Types Sbc and Sc

Figure 4 shows the distribution within κ -space for spiral galaxies of Hubble types Sbc and Sc (RC3 type numbers 4 and 5). The march of late-type galaxies away from the ZOE continues with this sample. The locus of Sbc–Sc galaxies within κ_1 – κ_2 parallels that of the earlier Hubble types, including the gEs and bulges. Within κ_1 – κ_3 and κ_2 – κ_3 , the Sbc–Sc’s generally follow the Sa–Sb’s.

When these data are merged with the Sa–Sb’s, we can see that early disk-dominated Hubble types Sa–Sc form a fundamental plane that is offset from and tilted slightly with respect to the DHG FP. The principal difference as a function of Hubble type is not the plane that each type defines, but rather the *distribution of galaxies within the plane*: later Hubble types are shifted to slightly lower masses and to lower surface brightnesses at a given mass.

4.6. Spiral Galaxies of Types Scd through Irr

Figure 5 shows the distribution within κ -space for spiral galaxies of types Scd to Irr (RC3 type numbers 6 through 10). Included in this diagram are the very large, very low surface brightness galaxies Malin 1 and Malin 2. In contrast to the earlier-type spiral galaxies and the gEs, these late type galaxies show essentially no correlation in either $\kappa_1-\kappa_2$ or $\kappa_1-\kappa_3$. However, their tilt in $\kappa_2-\kappa_3$ is now very pronounced in the sense of having lower κ_2 values for higher κ_3 . This tilt has erased all hint of correlation in the usual edge-on FP projection ($\kappa_1-\kappa_3$). In essence, $\kappa_2-\kappa_3$ replaces $\kappa_1-\kappa_3$ as the proper FP edge-on projection for late-type galaxies. Even though these galaxies show no correlation in $\kappa_1-\kappa_3$, their median M/L is still coincident with the DHG fundamental plane.

The properties of the two very large spiral galaxies Malin 1 and Malin 2 place them in unusual locations. Malin 2 lies close to the most massive end of the DHG FP in $\kappa_1-\kappa_3$, lies among late-type spirals in $\kappa_2-\kappa_3$, but has much higher mass than typical spirals. Malin 1 is even more massive with still lower surface brightness, larger radius and larger M/L . The positions of Malin 1 and Malin 2 within κ -space become more understandable when we discuss the properties of galaxy groups in § 5.

4.7. Quantifying the Interrelationships Among Galaxies in κ -Space

4.7.1. *The Distribution of Galaxies Relative to the ZOE*

The quantity

$$\delta_{2:1} \equiv \kappa_1 + \kappa_2 - 8 \tag{16}$$

measures the distance of a galaxy from the ZOE in $\kappa_1-\kappa_2$. Figure 6 shows histograms of $\delta_{2:1}$ divided by galaxy type. Median values, $\delta_{2:1}(\text{med})$, for each type of stellar system are shown in the figure. These histograms reinforce what we saw in the individual κ diagrams. The median values of $\delta_{2:1}$ show a steady progression along the Hubble sequence away from the ZOE, starting with $\delta_{2:1}(\text{med}) = -0.70$ for gEs, -0.90 for Sa galaxies, and through to -3.16 for Irr galaxies. For earlier Hubble types gE to Sbc, the histograms are reasonably Gaussian in shape, with similar widths and well defined means and medians. Sc galaxies have a bit wider histogram distribution, but $\delta_{2:1}$ is still reasonably Gaussian. From Scd to Irr galaxies, the distributions become progressively wider, with possibly large wings.

What if we had *not* made the K_1 correction to convert V_{rot} to σ_c , which amounts to

$\Delta\delta_{2:1} = -0.36$? In that case, Sa, Sab and Sb galaxies would be closer to the ZOE than the gEs, and the steady downward march through *all* Hubble types would be broken. The velocity-related K_1 correction, though small, seems necessary to properly rank-order the Hubble types.

4.7.2. *The Distribution of Galaxies Relative to the Fundamental Plane*

An analogous quantity

$$\delta_{3:1} \equiv \kappa_3 - 0.15\kappa_1 - 0.36 \tag{17}$$

measures the vertical distance of a galaxy in M/L from the DHG-defined fundamental plane (Equation 11). Figure 7 plots histograms of $\delta_{3:1}$ for Hubble types divided as in Figure 6. Unlike Figure 6, Hubble types here march first in one direction and then back again. Early Hubble types, gE–Sbc, move to lower M/L with advancing type. This probably reflects a greater number of young stars with later Hubble type. However, this trend begins to reverse at Sc, with later types marching back to *higher* M/L .

Several authors (Tinsley 1981, Faber 1982a, Verheyen 1997) have remarked on the higher M/L values of very late type galaxies in the B passband. However, this is the first time to our knowledge that the trend has been detected to set in as early as Sc. There are at least two factors that could contribute to this trend: 1) a tendency for more baryons to be in non-stellar form (i.e., H I and H₂ gas) in later types, and 2) more DM relative to baryons within the optical radius. We return to this issue briefly in §6.1.

4.7.3. *The Distribution of dE’s versus Scd–Irr Galaxies*

We have seen that each Hubble type occupies a distinct region of the κ_1 – κ_2 plane, with some overlap between neighboring Hubble types. Exceptions are the dEs and Scd–Irr galaxies, whose loci lie squarely on top of one another. This means that their masses and radii are similar, though the mass-to-light ratios of dEs are higher by roughly a factor of five at a given mass. In B²F1 we noted that dEs do not seem to be evolutionarily linked to giant DHGs because known evolutionary processes — tidal stripping, ram-pressure stripping, mergers, galactic winds — all move them in wrong directions in κ_1 – κ_2 . However a structural link with Scd–Irr’s seems plausible. If gas were removed from small late-type galaxies, causing star formation to slow or cease, and if the remaining stars faded, the

general location and high M/L 's of the dEs in κ -space might be explained. Several authors have suggested mechanisms that might strip gas from the shallow potential wells of small late-type galaxies via stripping, winds or “harassment” in clusters of galaxies (e.g., Lin & Faber 1983; Dekel & Silk 1986; Moore et al. 1996).

4.7.4. A Dissipation Strip in κ -Space?

As noted in B²F1, isotropic DHG galaxies (mostly lower-luminosity gEs) tend to be found in a narrow strip in κ -space parallel to the κ_2 axis and with boundaries $\kappa_1 = 2.7$ ($M_e \approx 10^{9.5} M_\odot$) and 4.3 ($\approx 10^{11.75} M_\odot$). Interestingly, among the 511 spiral galaxies in our sample, only 21 galaxies, all of Hubble type Sdm or Irr, lie more than 0.2 dex to the low mass side of this range, and only 4 spiral galaxies lie 0.2 dex or more to the high side. In other words, nearly all disk galaxies lie in the same mass range as the *isotropic* DHGs. Isotropy among DHGs implies flattening by high rotation. This, plus their high central densities (Faber et al. 1997) and probable oblate shapes (Tremblay & Merritt 1996) points to significant gaseous dissipation. Perhaps this strip in κ -space, $M_e = 10^{9.5} - 10^{11.75} M_\odot$, is the range of mass in which baryonic dissipation results in a flattened, rotating galaxy.

4.8. The Tully-Fisher Relation in κ -Space

A generalized TF relationship can be expressed as $\log L_e = A_C \log V_{rot}$, where A_C represents the color-dependent exponent in the standard TF power law. Using the relations defined in Appendix A we can rewrite this as

$$\left[\frac{4 - A_C}{\sqrt{2}}\right] \kappa_1 - \frac{A_C}{\sqrt{6}} \kappa_2 - \frac{A_C + 6}{\sqrt{3}} \kappa_3 = \text{constant}. \quad (18)$$

This is the equation of a plane in κ -space. We have already discussed the planar distribution of spirals and likened it to the fundamental plane for DHGs, which it resembles except for a slight tilt.

If $A_C = 4$ (i.e., $L_e \propto V_{rot}^4$), the coefficient of $\kappa_1 = 0$ and we get the simple relation $\kappa_3 \propto -\frac{1}{2.5\sqrt{2}}\kappa_2 = -0.283\kappa_2$. This plane is parallel to the κ_1 axis and projects with minimal scatter onto κ_2 - κ_3 . We have already noted the small scatter of spirals and Irr's in κ_2 - κ_3 , so the real spiral fundamental plane cannot be far from this line. If $A_C = 3$, $\kappa_1 - \sqrt{3}\kappa_2 - 3\sqrt{6}\kappa_3 = \text{const}$, which is a tilted plane that does not project perfectly to a line on any pair of κ axes.

The TF relation defined by our spiral and irregular galaxy sample is given in Figure 8. Part of the large scatter in this diagram comes from ignoring peculiar motions (cf. Faber & Burstein 1988). Nevertheless, it is evident that a relation of the form $-2.5 \log L_e \propto -7.5 \log V_{rot}$ defines this TF relation well, which implies $A_C = 3$. A formal fit yields $-2.5 \log L_e \propto -7.6(\pm 0.23) \log V_{rot}$ for all spirals and irregulars taken together, with coefficients of 7.48 (± 0.1) for Hubble types Sa-Sc, and 8.70 (± 0.35) for later Hubble types.

In other words, the fundamental plane for DHGs and the TF relationship for spiral galaxies are basically the same thing — each is the virial plane for its galaxy type, illustrating a family of self-gravitating objects in dynamical equilibrium and illuminated by stellar populations with well behaved mass-to-light ratios that vary as power-law functions of the basic structural variables (cf. Faber et al. 1987). This fact has been implicit since Faber & Jackson derived $L \propto \sigma^4$ for gE galaxies and Aaronson et al. (e.g., Aaronson & Mould 1986) derived $L \propto V_{rot}^4$ for spiral galaxies. What was not clear until galaxies were graphed together in κ -space is that the physical properties of spirals are continuous with those of DHGs. Indeed, DHGs define but one fundamental plane within κ -space; early-type spirals define another, and late-type spirals yet a third. In reality, there is probably a continuum of fundamental planes, just as we know there is a continuum of Hubble types, but we simplify them here to just three.

If observational errors and inconsistencies in the defined system of structural parameters are not important, and if galaxies are truly in gravitational equilibrium, then the existence of multiple FPs *must* reflect differences in mass-to-light ratios. This becomes obvious when one considers the *purely dynamical* version of fundamental plane space (σ, r, Σ) where mass surface density (Σ) replaces surface brightness. Since $\Sigma \propto M/r^2$ and since the virial theorem says that $M = V^2 r / G$, it is clear that there can be only one such plane. However, we cannot observe Σ independently of σ and r_e , so we replace it with the next best parameter, I_e , which we *can* observe. The two are related by $I_e \propto \Sigma(M/L)^{-1}$, which introduces a new wild card, mass-to-light ratio. It is the systematic variation in M/L as a function of σ and r for the different Hubble types that creates the multiple fundamental planes.

If we derive a three parameter, “FP-like” fit for the spiral and irregular galaxies we get $\log V_{rot} \propto 0.61(\pm 0.02)r_e + 0.39(\pm 0.02)I_e$ for the whole sample, with coefficients $(0.85 \pm 0.05, 0.57 \pm 0.03)$ for spirals Sa-Sc, and $(0.54 \pm 0.03, 0.34 \pm 0.02)$ for late-type galaxies. Errors were estimated using a bootstrap method using different subsamples of half the data at a time. These coefficients are to be compared with the usual values for the gE FP, $(0.72 \pm 0.07, 0.67 \pm 0.07)$, derived, as for example, by Faber et al. (1987). As we can see, the FP defined by the early-type spiral galaxies is reasonably consistent, within errors, with that of gE galaxies. In contrast, the FP defined by late-type galaxies is somewhat flatter. In both

cases, the fits confirm what we see in the figures.

5. Galaxy Groups, Galaxy Clusters and Globular Clusters in κ -Space

5.1. Groups and Clusters

To examine the κ parameters of galaxy groups and clusters, we shift the center of the volume to larger masses (higher κ_1), lower mean surface brightnesses (lower κ_2) and higher mass-to-light ratios (higher κ_3). Figure 9 shows such a plot of κ parameters for galaxy groups and clusters together with the giant spirals Malin 1 and Malin 2.

Galaxy groups are harder to identify uniquely than galaxies or galaxy clusters. Care must be taken to verify that groups defined in redshift space have properties that are similar to the “pure” groups one would have identified without contamination, redshift smearing, and projection biases. This issue is addressed using N-body simulations in Appendix B.

As pointed out by Schaeffer et al., rich clusters define a fundamental plane that is parallel to but offset from that of DHGs. This can be seen in Figure 9, where their projection in κ_1 – κ_3 is remarkably tight (large black dots). Galaxy groups define a second plane that is canted at a relatively steep angle to that of both the rich clusters and the giant ellipticals, bridging the two parallel planes between the high-mass galaxy end and the low-mass cluster end.

To quantify this picture, we calculate values of the M/L residual $\delta_{3:1}$ (Equation 17) for rich clusters and galaxy groups, the latter divided between spiral-rich and elliptical-rich groups and between groups with 10 or more galaxies versus 9 or fewer. Histograms of $\delta_{3:1}$ are shown in Figure 10, with the histogram for gE galaxies from Figure 7 included for reference. Figures 9 and 10 suggest some important conclusions about the physical properties of different kinds of groups and their relationship to galaxies:

1) The fundamental plane for rich clusters is parallel to that of DHGs but offset in κ_3 by 0.54 dex, or nearly a factor of 10 in mass-to-light ratio. Roughly 1/3 of this effect is due to the higher fraction of X-ray gas in clusters (Mushotzky 1991), which does not shine in B light, and the rest is due to the greater DM enclosed in clusters. Remarkably, the 16 rich clusters define a fundamental plane that is, if anything, *narrower* than the plane defined by bright elliptical galaxies.

2) The fundamental plane for galaxy groups is not a plane but a curved surface. For populous E-rich groups, this surface is nearly coincident with the plane for rich clusters, tilting down to lower M/L values for sparsely-populated S-rich groups. Yet rich groups,

poor groups, E-rich groups and S-rich groups all define κ -space distributions that are seen edge-on in κ_1 – κ_3 . The 10 groups that lie significantly high in M/L fall into two categories: groups within the Local Supercluster whose distances are underestimated at a level $>100\%$ by large-scale motions; and probable spurious and/or under-sampled distant groups with very large velocity dispersions. It is possible that the abnormally high M/L for these few groups are artifacts.

3) The low-mass end of the distribution of galaxy groups in κ -space intersects the high-mass end of the DHG FP for individual galaxies. It seems strange that the M/L for groups, which enclose DM, should be the same as that for galaxies, which are dominated by stars. However, the masses of low-mass groups are potentially afflicted by bigger observational errors due to projection effects and small-number statistics. Note that errors in the virial masses tend to move groups along a direction roughly parallel to the FP for low mass groups, as shown by the arrow in κ_1 – κ_3 in Figure 9. The effect of errors on the parameters of small groups is discussed further in Appendix B using N-body simulations. Errors may contribute some portion of the different tilt of low-mass groups. However, even factor of two errors in σ_e are not nearly enough to produce the full distribution of groups, so we conclude that most of the effect appears to be real.

4) Groups and clusters obey the same $\kappa_1 = -\kappa_2 + 8$ ZOE defined by the DHGs. The richest clusters appear to have high enough mean surface brightnesses to bring their κ_2 values up to this line, while the N93 groups show an upper boundary roughly parallel to, but offset below this line. This difference may be a richness effect caused by sampling different volumes — the Schaeffer et al. sample is drawn from a much larger volume than the CfA1 groups, and it is likely that the CfA1 volume is too low to include any large clusters.

5) Within κ_1 – κ_2 , rich clusters and rich groups define a loose relationship that projects nearly perpendicularly to the ZOE, paralleling the distribution of dwarf DHGs and Scd–Irr’s but at greater masses and fainter surface brightnesses. Like the late-type spiral galaxies, the distribution of small galaxy groups in κ_1 – κ_2 is amorphous. Some of the scatter for the small groups may stem from small-number statistics and projection effects.

6) Most E-rich groups (circles) are separated from S-rich groups (triangles) by a line that is roughly parallel to, but offset from, the ZOE in κ_1 – κ_2 . Just as galaxies march away from the ZOE at later Hubble types (Sec 4.7.1), so groups march away as the fraction of their late-type galaxies increases.

7) The “dissipation strip” previously defined for galaxies (§ 4.7.4) ends at $\kappa_1 \sim 4.3$. This is also a reasonable lower bound to the mass of groups, as expected since groups here

are explicitly identified by only their galaxies.

8) The κ parameters of the galaxy Malin 1 place it at the low-mass end of groups. Malin 2 is similar but closer to the gap between galaxies and groups. The structural parameters of these galaxies suggests that they may be “failed groups,” as we termed them in B²FN. By that, we mean systems in which baryonic dissipation and infall was so slow that the process of galaxy formation was interrupted by the formation of a “group.” Such events are evidently rare.

5.2. Globular Clusters and an Overall View of κ -Space

Globular clusters are included in the catalog because they are the oldest objects in our Galaxy, with some perhaps having formed “primordially” before the Galaxy as a whole collapsed. Globulars are also self-gravitating, and it is our desire to consider all self-gravitating stellar systems together. To view all stellar systems in one graph, we must collapse the scale down to such an extent that, for any reasonable symbol size, the points merge together to form an inky blob. Such a view of κ -space is given in Figure 11, which shows globular clusters relative to those of other stellar systems. They are separated from larger systems by a large gap, being denser and much less massive. Previous work (e.g., Schaeffer et al. 1993; Djorgovski 1995) has shown that the physical properties of globular clusters tend to project them along a fundamental plane parallel to but offset from that of DHGs. This is shown in Figure 10, which shows the histogram of $\delta_{3:1}$ values for the 51 globular clusters in our sample.

Globular cluster distances are determined in a manner that is largely independent of the assumed Hubble constant. If the assumed distance scale for globular clusters is systematically different from our cosmic scale (based on $H_0 = 50 \text{ km sec}^{-1} \text{ Mpc}^{-1}$), the difference will show up as a spurious offset most evident in κ_1 – κ_3 . The mean value of $\delta_{3:1}$ for the globulars is +0.26 dex (Figure 10). If $H_0 = 80 \text{ km sec}^{-1} \text{ Mpc}^{-1}$, $\delta_{3:1}$ would be reduced to +0.14 dex (cf. Nieto et al. 1990).

The distribution of globular clusters in κ -space seems more linear than planar. This line is most clearly seen in κ_1 – κ_2 but can also be seen in κ_2 – κ_3 . The κ -space distribution of globular clusters is more line-like than that of any other stellar system.

Many formation mechanisms have been suggested for globular clusters, including collapse from primordial fluctuations (Peebles & Dicke 1968; Rosenblatt et al. 1988), cooling flow thermal instabilities (Fall & Rees 1985), merger-induced shocks (Holtzman et al. 1992; Ashman & Zepf 1992), and molecular cloud collapse within galaxies (Searle &

Zinn 1978). Evidence from detailed examination of Galactic globular clusters suggests that, regardless of formation mechanism, only those clusters with long evaporation times and large perigalacticon distances survive today. Evaporation and potential shocking whittle away at an initial distribution, selecting as survivors only those clusters within a narrow range of *radii* (Gnedin & Ostriker 1997). This is consistent with the distribution of globular clusters in Figure 11, which is elongated and tilted with a zero point that corresponds to the predicted radius of 1-10 pc (cf. Figure 15).

6. κ -Space and Hierarchical Clustering

We turn now to a comparison of the topology of stellar systems in κ -space with the predictions of structure formation by hierarchical clustering. Figure 11 can be summarized by saying that the κ -space distributions of common stellar systems are viewed mostly edge-on in κ_1 - κ_3 , mostly face-on in κ_1 - κ_2 , and at intermediate angles in κ_2 - κ_3 . Each kind of stellar system defines a slightly different FP in this diagram, though they are all related. We suggest the term *cosmic metaplane* for this ensemble of continuous interlocking, and mainly parallel fundamental planes.

In retrospect, the existence of the metaplane is not surprising. We know from DHGs that any constraint of the form $M/L = f(M)$ will force a plane that is edge-on in κ_1 - κ_3 . The existence of the metaplane reflects the empirical fact that M/L is closely constrained by an object's mass. In the case of galaxies, this implies the known fact that galaxies of a similar Hubble type and size make stars in similar fashion. In the case of galaxy clusters, we can now add an additional requirement that clusters of a given mass have similar stellar baryon fractions. The physics behind these constraints is still unknown, especially the physics of star formation. However, the net result is that M/L varies by at most 100 over a mass range of $10^9 M_\odot$, and the range in M/L at any given mass is less than 10. It is this weak overall variation and local tightness in M/L that creates the metaplane.

However, for the purpose of understanding structure formation, the face-on view of the metaplane as seen in κ_1 - κ_2 is more useful than the edge-on view in κ_1 - κ_3 because of the information it contains on radii and densities. It is clear from Figure 11 that the properties of galaxies and clusters are highly organized and interrelated in κ_1 - κ_2 , and there appears to be a wealth of information on how structure formed. In this section we consider the distribution of objects in κ_1 - κ_2 in light of the prevailing paradigm for structure formation involving hierarchical clustering and merging (hereafter HCM).

6.1. Galaxies versus Clusters of Galaxies in κ -Space

The present comparison to data is similar to the approach taken by BFPR, expanded to the full 3-D κ -space and incorporating our newer and more extensive database for galaxies and clusters. The top hat spherical dissipationless collapse model for fluctuations is assumed (Gott & Rees 1975). If the fractional overdensity of a spherical fluctuation in a sphere of mass M is $\delta \equiv \delta\rho/\rho$ at redshift z , then the equilibrium radius of the collapsed dark halo formed from this fluctuation is (Faber 1983):

$$R_{dh} = 0.79 M_{12} \delta^{-1} h^{-2/3} \Omega^{-1/3} (1+z)^{-1} \text{ Mpc}, \quad (19)$$

where M_{12} is the mass in units of $10^{12} M_{\odot}$. This expression contains two independent parameters, δ and M_{12} , which, when varied, generate a two-dimensional family of collapsed objects that populate the *cosmic virial plane*. As previously noted, this is the parent plane for all the observed individual fundamental planes. The injection of different M/L rules for different families of objects at different locations transforms the virial plane into the collection of observed, interlocking fundamental planes that we have called the cosmic metaplane.

The cosmic virial plane is infinite in extent, defined by the ensemble of all possible collapsed objects of all masses and radii. In the real universe, this plane is only partially filled by the actual clustering process. The challenge of any theory of structure formation is to reproduce the observed distribution of objects versus mass and radius in this plane, i.e., to populate the plane with the right numbers of objects in the right places. Furthermore, to compare with observations, one must calculate *observed* radii for galaxies, which involves a theory of angular momentum generation and dissipation for these objects. Finally, to reproduce the full distribution in a κ -space defined by the B passband, a theory for M/L is needed, and thus a theory for converting baryons into B-band starlight.

We do not possess knowledge of all of these ingredients at this time. Nevertheless, schematically it appears that the distribution of objects in κ -space is broadly consistent with the predictions of HCM. To see this, we focus on κ_1 - κ_2 to take advantage of the radii information there. We also omit globular clusters, since how or whether they formed from primordial density fluctuations is unclear.

Since objects with higher overdensity collapse first in an expanding universe, clustering starts with the mass that has highest δ . Realistic density fluctuation spectra (e.g., Cold Dark Matter and its variants) decline monotonically with mass, so that clustering starts with small, high-density seeds of mass $\sim 10^7 M_{\odot}$ (BFPR) and progresses to form larger

masses of lower density. At any epoch, one expects to find a broad range of densities for collapsed objects at fixed mass, reflecting the fact that the initial overdensity δ of an individual sphere of mass M can vary widely.

The observed distribution of objects in κ_1 – κ_2 is consistent with this picture. The broad swath of points from upper left to lower right represents the collection of objects that have collapsed to date. Clustering started at the upper left at small masses and is progressing to the lower right. The total vertical width of the swath in κ_2 at fixed mass κ_1 corresponds to a factor of about 20 in radius. This is roughly consistent with expectations for an initial spectrum of Gaussian random fluctuations, as we show below. The division between galaxies and clusters of galaxies is a vertical line at $5.6 \times 10^{11} M_\odot$ (corresponding to $\kappa_1 = 4.3$; § 4.7.4). Since $5.6 \times 10^{11} M_\odot$ is the mass of a big galaxy and it takes at least three galaxies to make a group, the location of this line is not surprising.

However, in a deeper sense, the division between galaxies and clusters marks the boundary of baryonic dissipation: galaxies (for the most part) are objects in which global baryonic dissipation has occurred and to a large extent, groups and clusters are objects in which it has not. Thus, explaining why this line is located exactly where it is and why it appears to be *vertical*, i.e., at fixed mass, requires a full theory of dissipation, which is beyond the scope of this paper. In a general way, the location of this line probably reflects the well known boundary for gaseous ionized spheres that can cool before being incorporated into the next level of the merging hierarchy (Rees & Ostriker 1977, BFPR).

Galaxies and clusters are separated in κ_1 – κ_2 with a clear gap between them. This is due to baryonic dissipation. To develop a schematic estimate of its effects, we assume that the dissipated baryonic mass per dark halo is $M_{bary} = f_{bary} M_{dh}$, where f_{bary} is of order 0.1 (BFPR), and that the baryonic radius after collapse is given by $r_{bary} = f_{bary} r_{dh}$. Use of the same factor, f_{bary} , in both formulae ensures that the rotational velocity of the collapsed baryons, V_{rot} , will approximately equal V_{dh} . This is correct for collapse within an isothermal dark halo and also fits our current models of galaxy rotation curves. We further assume that, for galaxies, the effective mass, M_e , is the same as M_{bary} . With these assumptions, M/L decreases by a factor of f_{bary} , while surface brightness I_e increases by f_{bary}^2 .

These estimates enable us to undo the effects of baryonic infall and reconstruct what galactic dark halos would look like if the presently visible light were distributed like the DM. Figure 12a shows an enlargement of κ -space focusing just the κ_{appa_1} – κ_2 plane for galaxies, groups and clusters. The arrow labeled “dissipative infall” represents the above infall model. Objects shrink in both mass and radius as a result of baryonic infall, and thus move in both κ_1 and κ_2 .

Figure 12b attempts to reconstruct the invisible dark halos of galaxies by sliding all galaxy points back along the above infall vector, assuming that $f_{\text{bary}} = 0.1$. If hierarchical clustering is continuous across the boundary from dissipational to dissipationless collapse, we expect the reconstructed dark halos of galaxies to merge smoothly with those of groups and clusters. The reconstructed galaxy halos have that property, confirming that the original gap between the two families was the result of dissipation.

Note that dissipative infall broadens the total range of masses that can be plotted in Figure 12. Many dark halos of galaxies have lost their separate identities after spawning galaxies by merging with other halos (the so-called “overmerging” phenomenon, Katz & White 1993). Visible galaxies also merge but much more slowly since their cross-sections are reduced by baryonic dissipation. Thus, Figure 12b, which plots both halo populations together, is broader in mass than the population of halos at any one time — many of the reconstructed galaxy halos no longer exist because they have since merged with other halos to form the dark halos of groups and clusters.

Is the general slope of the ZOE consistent with HCM? Figure 12b shows that a major factor in the slope is baryonic dissipation because, without it, the distribution of galactic halos and cluster halos is much flatter than the ZOE. To explore the slope more carefully, we attempt to calculate the offset of DHGs from E-rich groups and clusters in Figure 12a. Since both of these groups are on the border of the ZOE, understanding their offset from one another will fix its slope.

The calculated offset consists of three parts, which we treat as vectors. The first vector, V_1 , is the dissipation vector just calculated. The second vector, V_2 , is the slope of the density fluctuation spectrum between the mass of a typical DHG dark halo and an E-rich cluster, assuming that both types of object arise from the same n - σ fluctuation. The shift along this vector assumes no change in M/L . The third vector, V_3 , takes account of the fact that there is an extra diminuation in the surface brightness of clusters relative to galaxy halos owing to the fact that much of the baryons in clusters are in hot gas that never formed into galaxies.

To calculate V_2 , we need the density fluctuation spectrum over the mass range from DHG halos to E-rich clusters ($10^{12.5} - 10^{15} M_\odot$). We take a power-law spectrum of the form

$$\delta_{rms} \propto M^{-1/2-n/6}, \quad (20)$$

where δ_{rms} is the rms amplitude of perturbations of mass M at fixed, initial redshift. We choose the value $n = -1.8$, which fits the slopes of current candidate density fluctuation spectra over this mass range (e.g., CDM; BFPR). This yields $\delta_{rms} \propto M^{-0.2}$. After collapse,

the equilibrium structural properties of a dark halo that began with given δ_{rms} and M obey the relations (Gott & Rees 1975):

$$r \propto \delta_{rms}^{-1} M^{1/3}, \quad (21)$$

$$\rho \propto \delta_{rms}^3, \quad (22)$$

and

$$V \propto \delta_{rms}^{1/2} M^{1/3}. \quad (23)$$

Combining these with $\delta_{rms} \propto M^{-0.2}$ yields the scaling laws for a typical object versus mass:

$$r \propto M^{0.53}, \quad (24)$$

$$\rho \propto M^{-0.60}, \quad (25)$$

$$V \propto M^{0.23}, \quad (26)$$

and

$$I \propto M^{-0.07}. \quad (27)$$

assuming no change in M/L . These relations allow us to calculate the vector V_2 assuming $n = -1.8$.

The final vector V_3 requires us to estimate the extra diminuation in surface brightness of clusters relative to galaxy halos due to hot gas. We estimate this empirically by taking the total change in M/L between an average DHG galaxy and a typical E-rich cluster (taken to be 0.95 dex in κ_3 , or a factor of 44 in M/L , cf. Figure 11.). We then divide this by the factor due to dissipation (10, above), which leaves 4.4 due to hot gas. This is not far from the factor of 3 estimated from X-rays by Muzhotzky (1991). Vector V_3 affects surface brightness only, leaving mass unchanged.

The three vectors are shown in Figure 12a. Their components in κ -space units are: $V_1 = (0.71, -2.04)$, $V_2 = (1.79, -0.11)$, and $V_3 = (0.00, -1.05)$. Their sum is a little steeper than the observed ZOE, i.e., the surface brightnesses of E-rich clusters are a little higher than expected. This could reflect the fact that dissipation is a little smaller than the factor of 10 assumed, or that visible galaxies in E-rich clusters have condensed slightly relative to the DM by dynamical friction. Given the roughness of the calculation, the agreement is acceptable.

In closing this overview of structural properties, for completeness we plot three other parameter combinations that are often useful. Figures 13 and 14 are updates of plots in BFPR. The first plots baryon density from Column 19 versus virial temperature from Column 18 in Table 1, using the equations given in Appendix A. This combination is useful for assessing baryon cooling and dissipation, and the density axis (assuming similar collapse factors) is a measure of the redshift of collapse. The distribution of groups and clusters in this diagram is similar to that in BFPR, but the galaxies are different. The present distribution of galaxies is much more horizontal than the schematic, elongated representation in BFPR, with galaxies strung out at roughly constant density from right to left as a function of Hubble type.

The surprising conclusion from this graph is the roughly *similar density* of all Hubble types within r_e today. At face value, this implies similar collapse redshifts, an inference that could break down, however, if all galaxies did not have constant collapse factor f_{bary} (see below). Our use of stellar half-light radii also underestimates the baryonic radii of late-type galaxies, whose baryons are mostly H I. A switch to H I radii would move these galaxies to lower densities and later formation times. Finally, the present database is strongly biased against low-density, low-surface brightness galaxies, which also would appear higher (later) in the diagram. For all these reasons the apparent constancy of formation redshift for all Hubble types in Figure 13 may be exaggerated. Nevertheless, the present data are adequate to illuminate the early Hubble types, and for them the flatness of the locus in Figure 13 is striking.

Figure 14 plots velocity versus mass. This figure resembles the corresponding figure in BFPR more closely because this projection is a nearly edge-on view of the metaplane, and the distribution of points is therefore insensitive to the distribution of objects in the plane. The long loci of galaxies here are basically the Faber-Jackson and TF relations. There is clearly a similar relation for groups and clusters although it has never before received much notice.

Figure 15 is new here and plots radius versus mass. It is useful for estimating the radial collapse factor for galaxies due to baryonic dissipation. If we fit an $n = -1.8$ power-law

slope through the middle of the spiral-rich groups, compare to a similar locus through the middle of the spirals themselves, and demand that the shrinkage due to dissipation be the same in mass as in radius (i.e., both equal to f_{bary}), we find that an offset of a factor of 19 in radius and mass is required to account for the offset of spirals from spiral-rich groups in Figure 15. This value of f_{bary} is larger than the usual value of 10 assumed above, but the method is rough. The point is that Figure 15 provides another target to shoot at in matching the radii of galaxies versus groups.

6.2. Hubble Types and the Dressler Effect

We turn now to substructure within the galaxy and cluster subregions. The most obvious feature is the “banding” in κ_1 – κ_2 for galaxies, yielding the downward march of Hubble types away from the ZOE (Figure 6). A natural (but not unique) interpretation of this phenomenon was given by Faber (1982a) and BFPR in terms of forming different Hubble types from differing degrees of overdensity. The overdensity within a given sphere of mass M can be written

$$\delta = n \delta_{rms}(M), \tag{28}$$

where $\delta_{rms}(M)$ is the rms perturbation in spheres of mass M . Such a perturbation obeying Equation 28 is termed an “ n - σ ” perturbation. Equations 21–23 imply that families of perturbations with constant values of n form parallel lines in κ_1 – κ_2 , with higher n lying at higher κ_2 . The relation between n and the vertical offset $\delta_{2,1}$ is:

$$\Delta \log n = 0.41 \Delta \delta_{2,1}. \tag{29}$$

We can use this relation to infer relative values of overdensity n for each of the Hubble type bins in Figure 6. These values are tabulated in Table 2. Two normalizations have been used to convert to absolute n , one assuming that gEs are 3- σ perturbations as in BFPR, the other that Sc’s are 1- σ perturbations. The latter is more plausible since the predicted number of early-type galaxies is otherwise smaller than observed. Either way, the total range in n implied by $\delta_{2,1}$ by Equation 29 is about a factor of 10. Regardless of normalization, the implied overdensity for Irr’s is only 0.2 – 0.3, which is close to 0. These objects barely managed to collapse.

Notice that Equation 29 between $\delta_{2,1}$ and n is logarithmic, which means that, as n approaches 0, the ridgelines in Figure 12a march to $-\infty$ in κ_2 . The distribution of objects

formed from an ensemble of Gaussian random perturbations will therefore have a skewed distribution in $\kappa_1\text{--}\kappa_2$; the density of objects peaks around the 1- σ ridgeline and falls off above and below that due to the scarcity of high- σ peaks on the one hand and the spreading of low- σ peaks to large radii and low surface brightness on the other. These features are not yet quantifiable with the present data because they are not volume limited. However, the observed distribution does broadly show the sharp upper envelope and tail to low $\delta_{2:1}$ that are expected.

The logarithmic relation between n and $\delta_{2:1}$ in Equation 29 may explain the variable widths of the distributions observed for different Hubble types in $\delta_{2:1}$. If each Hubble type were selected from approximately equal intervals in n , it would appear in $\kappa_1\text{--}\kappa_2$ with progressively wider widths for lower values of n . This may help to account for the relatively tight loci of early Hubble types versus the wide, amorphous loci of the later types.

The above discussion implicitly assumes all galaxies have the same radial baryonic collapse factor, f_{bary} and overdensity n is the sole determiner of Hubble type. This may be termed the “density hypothesis” (Faber 1982a). An alternate picture is f_{bary} varies with Hubble type. The simplest way this might happen is if the dark-halo angular momentum parameter $\lambda \equiv LE^{1/2}G^{-1}M^{-5/2}$ (Peebles 1969) is not constant with Hubble type. If baryonic collapse is halted by angular momentum (Fall & Efstathiou 1980), more slowly rotating halos will collapse further. If λ alone were the determining factor for Hubble type, early-type galaxies would descend from slowly rotating, low- λ dark halos because they are denser at a given mass than late-type galaxies, while late-type galaxies would come from rapidly rotating halos. The dissipational collapse factor f_{bary} would then determine Hubble type. Faber (1982a) termed this the “dissipation hypothesis”, but a better term might be the “ λ -hypothesis.”

Since the density hypothesis fits many features of the data, there is no compelling reason at the present time to invoke λ variations. N-body simulations of dark halos have furthermore failed to reveal any strong correlation between λ and environment, as would be needed to explain the high density of early-type galaxies in clusters (Barnes & Efstathiou 1987). However, *very* low-surface-brightness objects are under-represented in the present data set. If they were taken into account, the total spread of galaxies in $\delta_{2:1}$ would be larger, and there would be more reason to invoke λ , at least as a second parameter. Higher λ in later-type galaxies would cause them to collapse less, leading to more DM within their baryonic radii (Tinsley 1981, Faber 1982a, Verheyen 1997). Excess DM would tend to suppress spiral structure (Toomre 1964, 1981; Binney & Tremaine 1987) in later Hubble types, producing Irr’s as observed. On balance, it would seem timely to re-examine the λ -versus density- hypotheses using the newer simulations that model baryonic dissipation

more accurately. It is of course possible that both λ and initial overdensity are play a role in determining Hubble type.

Turning now to groups and clusters, we note a parallel banding effect that matches the Hubble type bands among galaxies. The analog to Hubble type is mean group Hubble type and, as previously noted, there is a strong tendency for early-type-dominated groups to lie close to the ZOE and for groups to become progressively late-type-dominated away from this line. This is simply the “Dressler effect” (Dressler 1980, Postman & Geller 1984), wherein the Hubble type of a galaxy is strongly correlated with its environment — early types are found preferentially in dense regions, while late types are found in sparse regions. The origin of this effect is probably that realistic density fluctuation spectra are flatter than white noise, with the result that density fluctuations on neighboring scales are correlated (BFPR; Bardeen, Bond, White, & Efstathiou 1988). The high- σ peaks that spawn early-type galaxies (in the density hypothesis) are statistically embedded in high-peak clusters (BFPR), which also collapse to high density and lie near the ZOE. This effect has been born out by N-body/hydro simulations (e.g., Cen & Ostriker 1994).

6.3. The Slope of Hubble Types within κ_1 – κ_2

So far the HCM theory of structure formation is adequate to account for most of the broad features of structures in κ -space. We now highlight one aspect of the data that has so far eluded explanation. The question at issue is the *slope* of the galaxy loci for individual Hubble types in κ_1 – κ_2 . We have seen in Figures 1–6 that this slope follows the ZOE. We were able to account for the slope of this line *between galaxies and clusters* by assuming an $n = -1.8$ power-law coupled with plausible dissipation. However, the simplest theory would say that dissipation and overdensity (n) are *both constant within a given Hubble type*. Each type should therefore parallel the density fluctuation slope (vector V_2 in Figure 12b). This is much shallower than the observed loci for Hubble types.

Let us review exactly what the vector V_2 means. It is the predicted slope for a collection of objects formed from a power-law initial density fluctuation spectrum with slope $n = -1.8$, constant n - σ overdensity, constant M/L , and constant radial baryonic collapse factor, f_{bary} . Since the observed slope does not match this prediction, one or more of these assumptions must be wrong. M/L is constrained to vary only modestly by observations, and the constant slope and overdensity of a given Hubble type are attractive assumptions we are wanting to test. That leaves $f_{bary} = \text{constant}$, which is perhaps the least secure assumption. In words, the radii of big galaxies within each Hubble type seem to be larger than predicted by the constant collapse picture — big galaxies are more diffuse

than expected.

This problem was first highlighted for DHGs by B²F1 but now appears to affect *all* Hubble types through at least Sc. What is needed in the constant collapse picture is to either halt the collapse of the baryons at larger radii in the first place or reinflate them to larger radii later. The extension of the problem to disk-dominated galaxies is thus very significant. Pressure-supported DHGs can be inflated by simply adding energy, for example by heating their stars through mergers in dense groups. However, increasing the radii of *disk* galaxies is not as easy — it requires adding angular momentum as well as energy. This cannot be done through mergers without destroying the disks. Thus, the process, whatever it is, must take place for disk galaxies while the material is still gaseous, which adds an important constraint.

To summarize, understanding the existence of the ZOE involves two separate phenomena. One issue is the slope of the line between galaxies and clusters, and that seems explicable using HCM together with plausible dissipation. The other is the slope of individual Hubble types themselves. This problem has no easy solution at the present time. Is the existence of one, smooth ZOE an accident, or is it fundamental? Whatever the answer, matching galactic radii as a function of mass and Hubble type is one of the most pressing targets for galaxy simulations.

6.4. Mass-to-Light Ratios of Groups and Clusters

A final puzzle concerns the pronounced increase (and curvature) in κ_3 vs. κ_1 (M/L vs. M) for groups and clusters (see Figure 9). An offset of groups and clusters to higher M/L than galaxies is expected because the latter contain more DM. However, this offset does not appear suddenly in going from galaxies to groups, as one might have expected, but rather sets in as a gradual rise in M/L vs. group size.

The Cold + Hot Dark Matter (CHDM) simulations of Nolthenius, Klypin, & Primack (1997; hereafter NKP97) may help to explain part of this effect. The apparent overlap in M/L between small groups and galaxies may be caused the large errors of small groups due to small-number statistics and projection effects. Appendix B compares M/L 's for redshift-selected small groups vs. the same groups selected in real space (Figures 16a and 16b). The lower M/L values of the former overlap with the M/L 's of galaxies, while the latter do not. The locus for the simulation redshift-selected groups is also steeper at the faint end and follows the mass-error trajectory. The same effect is seen in the real groups. The simulations thus suggest that errors may be obscuring a real discontinuity in M/L

between galaxies and small groups and creating the appearance of a smooth trend. On the other hand, the fact that Malin 2 lies on the gE FP, while Malin 1 lies within the group M/L for its M suggest that these very rare kinds of galaxies can bridge this gap.

This effect cannot produce a second and more important trend — the striking overall *rise* in group M/L as a function of mass. Remarkably, the same effect is seen in the simulations as well as the real data (Figure 9 vs. Figures 16a and 16b). Tests show that the effect persists for “break-up” vs. “no-break-up” group catalogs, and for real-space vs. redshift-space selected groups. It is not due to a decrease in the average luminosities of galaxies in large groups (this effect is 20-30% at most, Appendix B) but rather to an actual decrease in the number of galaxies identified in large clusters. As we emphasize in that Appendix, the simple prescription used for identifying and illuminating galaxies in these pure dissipationless simulations should be adequate only for comparing the properties of groups selected in redshift space to their counterparts selected in real space. Even so, the match to the N93 groups is good enough that it’s tempting to wonder whether the simulations may yet capture more truth than one might at first suppose. In addition, it remains unresolved why the slope of M/L for large groups so closely matches that for DHGs (the two planes are parallel, cf. Figure 10). All-in-all, there are several important unanswered questions concerning the M/L ’s and galaxy formation efficiency in groups and clusters.

6.5. Guidelines for Future Comparisons to Simulations

It is our hope that the present database (and its descendents) will be of use to modelers attempting to simulate galaxy formation and other types of structure in the universe. In assembling the present data, we have taken the easy path of sticking close to raw observations with a minimum of transformations to more fundamental quantities. This has the virtue of minimizing present uncertainties but forces future simulations to be more complete and realistic. Here is a reminder of the basic properties of the present data:

- 1) All luminosities are B-band light emitted by stars.
- 2) The effect of interstellar extinction in our Galaxy is fully corrected for, but the extinction correction for internal extinction corrects galaxies only to face-on. The correction from face-on to fully-corrected is not well understood and depends on both the ratio of absorption to scattering for dust grains and their distribution in the galaxy relative to the stars. If forward scattering by dust is dominant, face-on luminosities may even be too bright.

3) Radii are half light radii defined by starlight in the observed B-band light profile. No adjustments are made for variable extinction with radius.

4) The central line-of-sight velocity dispersion for a hot system, σ_c , is adopted as the fundamental definition of velocity. Effective dispersions, σ_e , of groups and clusters and peak rotation velocities, V_{rot} , of disk systems are transformed to equivalent values of σ_c .

5) The basic finding list for galaxies consists of objects with the necessary data in the RC3. The sample is therefore quasi-magnitude limited and weighted to bright objects. Galaxies of low surface brightness are especially selected against.

Four physical processes must be modeled to permit comparison with this data set:

1) Stellar radii of galaxies must be determined. This requires a theory for the initial distribution of gas within the galaxy, plus a theory for its conversion to stars as a function of radius and time. The gaseous radii of disks depend on the fraction of baryons that have cooled by today, and from what radius they fell in (the collapse factor). This in turn depends on angular momentum generation in dark halos including the exchange of angular momentum between the baryons and DM and among the various baryonic components. Angular momentum transfer in mergers and in distant interactions also needs to be considered.

The stellar radii of DHGs depend on the radii of any previously formed stellar disks absorbed in mergers (Kauffmann, White, & Guiderdoni 1993), the relative timescales for infall versus star formation (Faber 1982b), mass loss in stellar winds, merger dynamics, and possibly other unknown factors.

2) B-band luminosities of galaxies must be computed. This requires the history of star formation at every location, including the stellar birthrate and initial mass function. Luminosity profiles and total luminosities need to be converted to observed face-on quantities by correcting for dust.

3) For disk galaxies, observed peak rotation velocity V_{rot} must be related to σ_e for the dark halo. This requires a theory for gas infall and the quasi-adiabatic simultaneous pulling-in of the DM particles.

4) For groups and clusters, the main uncertainty is what fraction of baryons is converted into stars and how this varies as a function of local galaxy density. There may also be radial or other segregation effects between galaxies, hot gas, and DM.

7. Conclusion

In this paper we have extended our view of κ -space to include all major types of equilibrium, self-gravitating systems in the local universe. To do this, we have developed consistent definitions of luminosity, radius, surface brightness, and internal velocity. Internal velocities in particular require special transformations to achieve uniformity among the different types of galaxies. When these corrections are applied, a pleasing continuum of physical properties is evident among galaxies of all Hubble types from giant ellipticals to Sd and Irr galaxies.

Each type of stellar system is found to populate its own fundamental plane in κ -space. Six different planes are found: 1) the original fundamental plane for DHGs; 2) a parallel plane slightly offset for Sa-Sc spirals; 3) a plane with different tilt but similar zero point for Scd-Irr galaxies; 4) a plane parallel to the DHG plane but offset by a factor of 10 in mass-to-light ratio for rich galaxy clusters; 5) a plane for galaxy groups that smoothly bridges the gap between rich clusters and galaxies; and 6) a plane for Galactic globular clusters. We propose the term “cosmic metaplane” to describe this ensemble of interrelated and interconnected fundamental planes.

The projection $\kappa_1\text{--}\kappa_3$ (M/L vs. M) views all planes nearly edge-on. The $\kappa_1\text{--}\kappa_2$ projection views all planes close to face-on, while $\kappa_2\text{--}\kappa_3$ shows variable slopes for different groups owing to the different tilts of the individual planes. No stellar system yet violates the rule first found from the study of DHGs, namely, $\kappa_1 + \kappa_2 < 8$, which we term the “zone of exclusion,” or ZOE. In physical terms, this implies that the maximum global luminosity volume density of stellar systems varies as $M^{-4/3}$.

Each Hubble type defines a band in $\kappa_1\text{--}\kappa_2$ parallel to the ZOE. Hubble types march monotonically away from the ZOE, with DHGs being closest and Sd–Irr’s most distant. This reflects a decrease in the average mass and surface brightness along the Hubble sequence. The Tully-Fisher relation ($L \propto V_{rot}^{3-4}$) is simply the proper compromise projection to view the spiral-irregular planes close to edge on, analogous to the $D_n\text{--}\sigma$ relation for DHGs. All galaxy types, spirals/irregulars and DHGs, show the mutual dependence of characteristic velocity, effective surface brightness and effective radius that first characterized the fundamental plane (FP) for gE galaxies. The fact that the coefficients in these relationships differ somewhat among galaxies of different Hubble types again illustrates the fact that we are not dealing with just one FP, but several interlocking ones that form a cosmic metaplane.

The rich clusters originally studied by Schaeffer et al. (1993) define yet another fundamental plane that is remarkably tight and parallel to that of the DHGs but offset by

a factor of 10 higher in mass-to-light ratio. The galaxy groups of Nolthenius (1993) likewise define a fundamental plane, but one that is tilted and appears to link the FPs for rich clusters and for DHGs. Some fraction of this tilt is due to errors in group properties due to small number statistics and chance projection effects, but most appears to be real. Just as the loci of Hubble types march steadily away from the ZOE along the Hubble sequence, the mean location of groups marches away from the ZOE with increasing spiral content. This is the well known Dressler (1980) effect. The two large diffuse galaxies known as Malin 1 and Malin 2 have physical properties similar to those of spiral-dominated galaxy groups.

Globular clusters distribute themselves within κ -space close to the DHG fundamental plane (cf. Djorgovski 1995; Schaeffer et al. 1993) but offset in zeropoint. They occupy a small band of radii, as predicted if the present population of clusters were a small surviving subset of a larger, broader population.

In broad-brush strokes, the distribution of galaxies, galaxy groups and galaxy clusters within κ -space can be understood as the result of hierarchical clustering and merging from a power-law initial density fluctuation spectrum. The cosmic metaplane is simply the cosmic virial plane common to all self-gravitating equilibrium stellar systems, tilted and displaced in mass-to-light ratio by different amounts in different regions due to differences in stellar populations and amount of baryonic dissipation. Hierarchical clustering from an $n = -1.8$ power-law density fluctuation spectrum (plus dissipation) comes close to reproducing the slope of the ZOE. The progressive displacement of Hubble types from this line is consistent with the formation of early-type galaxies from higher n - σ fluctuations than later Hubble types.

A major mystery is why the slopes of *individual* Hubble types in the κ_1 - κ_2 plane parallel the ZOE. At face value, this appears to suggest *less* dissipation of massive galaxies within their dark halos compared to lower-mass galaxies of the same Hubble type. A second mystery is the behavior of M/L vs. L for groups and clusters. Two slopes are seen, both tight, with group M/L 's climbing more steeply than clusters. The same general rise in M/L vs. M is seen in the simulations, but we have no good physical explanation either there or in the real data. The tightness in M/L implies a remarkably close coupling between the galaxy formation efficiency, stellar populations, hot gas content, and dark matter content of groups and clusters as a function of total mass.

We discuss the limitations of the present data and alert modelers to the large number of physical processes that need to be calculated in order to make a realistic comparison between these data and simulations. Use of the B band is an important limitation. One would ideally like to view the properties of these stellar systems in redder passbands less affected by dust and recent star formation. Also crucial is a volume-limited sample of

nearby galaxies, needed for an unbiased census of galaxies in κ -space.

We now realize that the initial discovery of the elliptical galaxy fundamental plane a decade ago was but the first glimpse of the full cosmic metaplane that is defined by the physical properties of all gravitationally-bound, star-defined systems. As with our first investigation of dynamically hot galaxies, κ -space has proved to be a valuable tool for exploring this “cosmic metaplane.”

The data used here are the result of the collected efforts of many astronomers over the years, as summarized in the catalog tables we have used. We thank Alberto Cappi for sending us the Schaefer et al. data in computer readable format, Giampaolo Piotto for pointing us the in right direction for the globular cluster data, and Anatoly Klypin and Joel Primack for use of their CHDM simulation. DB acknowledges partial support from NSF AST90-16930. SMF acknowledges support from NSF AST95-29008 and from NAS-5-1661 to the WFPC1 IDT.

A. Standard Quantities Derived from κ Parameters

In this Appendix we give convenient relations for transforming κ parameters into more familiar quantities. The fundamental plane parameters r_e , I_e and σ_c are related to the κ parameters as follows:

$$\log r_e = \frac{\sqrt{2}}{2}\kappa_1 - \frac{\sqrt{6}}{6}\kappa_2 - \frac{\sqrt{3}}{3}\kappa_3; \quad (\text{A1})$$

$$\log I_e = \frac{\sqrt{6}}{3}\kappa_2 - \frac{\sqrt{3}}{3}\kappa_3; \quad (\text{A2})$$

$$\log \sigma_c = \frac{\sqrt{2}}{4}\kappa_1 + \frac{\sqrt{6}}{12}\kappa_2 + \frac{\sqrt{3}}{6}\kappa_3. \quad (\text{A3})$$

With r_e in kpc and σ_c in km s^{-1} , we define $M_e = 4.65 \times 10^5 \sigma_c^2 r_e M_\odot$, where we have taken the standard Keplerian formula for defining the mass of a disk, $M_e = r_e V_{rot}^2 / G$, and corrected V_{rot} to σ_c as given by K_2 . This yields

$$\log M_e (M_\odot) = \log (\sigma_c^2 r_e) + 5.67 = \sqrt{2}\kappa_1 + 5.67. \quad (\text{A4})$$

With r_e in kpc and I_e in B-band $L_\odot \text{ pc}^{-2}$, the luminosity within the effective radius is defined as $L_e = \pi \times 10^6 I_e r_e^2 L_\odot$, resulting in

$$\log L_e (L_\odot) = \log (I_e r_e^2) + 6.50 = \sqrt{2}\kappa_1 - \sqrt{3}\kappa_3 + 6.50. \quad (\text{A5})$$

The B-band mass-to-light ratio within r_e is the ratio of these two:

$$\log [M_e / L_e] (\odot) = \log (\sigma_c^2 r_e) - \log (I_e r_e^2) - 0.83 = \sqrt{3}\kappa_3 - 0.83. \quad (\text{A6})$$

Our definitions of effective virial temperature, T_e , and mean baryon number density within the effective radius, $n_{bary,e}$, follow those of BFPR. For T_e we equate a Maxwellian distribution to a Boltzmann distribution, $3/2\mu m_p \sigma_e^2 = 3/2kT$, where m_p is the proton mass. Using a mean molecular weight $\mu = 0.6$ for ionized primordial H+He yields $T_e = 72.7 \sigma_e^2 \text{ K} = 51.4 \sigma_c^2 \text{ K}$, for σ in km s^{-1} . Thus

$$\log T_e (\text{K}) = \log (\sigma_c^2) + 1.71 = \frac{\sqrt{2}}{2}\kappa_1 + \frac{\sqrt{6}}{6}\kappa_2 + \frac{\sqrt{3}}{3}\kappa_3 + 1.71. \quad (\text{A7})$$

The baryon number density $n_{bary,e}$ is defined as $f_{bary}M_e/(4/3 \pi r_e^3 m_p)^{-1}$, where f_{bary} is the fraction of M_e contributed by baryons within the effective radius. The baryon correction is expressed as $s_{type} = \log f_{bary}$. In the present units,

$$\log n_{bary,e} (\text{cm}^{-3}) = \log (\sigma_c/r_e)^2 - 2.34 + s_{type} = -\frac{\sqrt{2}}{2}\kappa_1 + \frac{\sqrt{6}}{2}\kappa_2 + \sqrt{3}\kappa_3 - 2.34 + s_{type}. \quad (\text{A8})$$

Systems that are dominated by dark matter (DM) have significant baryon corrections. Examples are galaxy groups (Mulchaey et al. 1996), galaxy clusters (Mushotzsky 1991), and extreme dwarf spheroidals (B²F1), for which we assume $s_{type} = -1.0$. For dwarf ellipticals, we assume $s_{type} = -0.2$ (B²F1), and for spirals we also assume $s_{type} = -0.2$ dex (Rubin et al. 1985, corrected to r_e). All of these s_{type} corrections are likely to be within 0.3 dex of being correct, which is similar to the error that we make by assuming that all the mass is spherically distributed. Systematic errors of this size are of no consequence to our conclusions.

B. Using N-Body Simulations to Calibrate Group κ Properties

There are several well-known difficulties in linking galaxies in redshift space into true, physical associations with properly measured properties:

(1) As filamentary structures are usually comprised of a series of dense regions of galaxies, groups are often poorly separated from surrounding galaxies. This can lead to contamination from foreground and background galaxies.

(2) Group structure is often unrelaxed, so that local gravitational tidal fields from larger masses (say superclusters) can have a significant effect on the spatial and redshift distribution of galaxies within even a bound group.

(3) Groups generally have few bright, visible members, resulting in shot noise and random projection effects which can lead to substantial errors in determined quantities.

These problems require that a grouping algorithm be carefully calibrated against realistic simulations which include these effects. While based on the early Nolthenius & White (1987) simulations, the N93 link criteria have recently been shown to be near optimal (as defined below) by calibration with more recent N-body simulations (Nolthenius, Klypin & Primack 1994; NKP94; Nolthenius, Klypin & Primack 1997; NKP97), which use the simulations of Klypin, Nolthenius & Primack (1997). Our plan is to use versions of these

catalogs constructed to match the CfA1 Survey and compare κ -space properties in redshift space to those of groups selected in real space (i.e. using full 3D information).

B.1. Constructing Mock-Sky Catalogs

The Klypin et al. N-body simulation we use here evolves an $\Omega = 1$, 70%/30% mix of “Cold + Hot Dark Matter” (a CHDM model) on a 100 Mpc across 512^3 cell grid using a particle-mesh pure dissipationless code. Within this simulation, potential galaxies are identified as cells with local overdensity $\delta\rho/\rho > 30$. Since galaxies must be local overdensities, a centrally concentrated array of overdense cells will still be identified as only a single galaxy. We identify all ~ 30000 “galaxies”, generate an equal number of Schechter luminosities, and pair up the luminosities with galaxies so that luminosity rises monotonically with 1-cell mass.

We then select a “home galaxy” similar to our location in the real universe, observe the catalog and impose the CfA1’s $m_B = 14.5$ magnitude limit. Since “observing” is done after L ’s are assigned, large scale flows and Malmquist bias will lead to a steeper α and brighter M^* when observed in redshift space. The L assignment is therefore done iteratively until the redshift-space-observed luminosity function and the sky-projected galaxy density of the resulting catalogs both match that of the CfA1. To include possible edge effects yet maximize sample size, we include the full sky minus a 20 deg wide “zone of avoidance”, which includes roughly 9000 “galaxies” and 830 “groups”. See NKP97 for a more complete description of the construction of the sky catalogs.

We analyze here NKP97’s CHDM₂ simulation because both the fraction of galaxies in groups and the median group velocity dispersions closely match those of identically selected CfA1 groups not only at the optimal link parameters but throughout the entire range of links (NKP94, NKP97). NKP97 argue that these two properties are very sensitive to the spatial and velocity structure of galaxies on group scales, and therefore are the most appropriate indicators to match when attempting to design and calibrate an optimal grouping algorithm.

However, we strongly caution against identifying these objects with representative observed galaxies *in a CHDM universe*, for two reasons. First, with a cell size of 195 kpc, these simulations have neither the resolution nor the baryonic physics needed to model individual galaxies or even galaxy dark matter halos with confidence. Second, the dark matter halos in these simulations are affected by the overmerging problem (Katz & White 1993) and the proper way to “break up” these overmergers into galaxies is still

poorly understood. In fact, it is the un-broken catalogs which show the closest structural similarities to the real data and which we therefore use here. We also note that while the NKP97 “breakup” catalogs yield closely similar κ -space properties, it is quite possible the level of overmerging was underestimated (see NKP97 “ 2ν ” results). Our goal here is only to see how κ values change between real space and redshift space. We resist the temptation to judge the merits of CHDM as a cosmological model.

The redshift space link relations are described in N93 and NKP97. To select corresponding groups in real space we again seek to identify number density enhancements above a consistent density contrast, With 3D information, the N93 sky and redshift dimensions are now described by a single isotropic separation, which is again scaled to account for growing incompleteness at higher distance. Distances here assume a smooth Hubble law, and, unlike in N93, there has been no attempt to “fine-tune” groups in the densest regions. Thus, mock-galaxies at distance V from the observer are linked if their 3D separation is less than $D(V)_L$, defined by

$$\lambda(V) = \frac{L(V)_{\text{lim}}}{L^*} \quad , \quad (\text{B1})$$

$$R(V)_{\text{M.I.S.}} = [\Phi(V)]^{-1/3} = (\phi^* \Gamma [1 + \alpha, \lambda(V)])^{-1/3} \quad , \quad (\text{B2})$$

and

$$D(V)_L = D_0 R(V_0)_{\text{M.I.S.}} \left[\frac{\Phi(V_0)}{\Phi(V)} \right]^{1/3} . \quad (\text{B3})$$

Φ is the integrated galaxy luminosity function above the limiting luminosity $L(V)_{\text{lim}}$ visible at distance V due to the catalog apparent magnitude limit m_{lim} (Schechter 1976) with the usual parameters ϕ^* and α ; L^* is the luminosity corresponding to the Schechter luminosity M^* ; $\lambda(V)$ is defined as $10^{[0.4(M^* - (m_{\text{lim}} - 25 - 5 \log(V/H_0)))]}$; H_0 is the Hubble constant; Γ is the incomplete gamma function, $D_0 = 0.36$ is our link parameter, V_0 is an arbitrary scaling distance set to 1000 km sec^{-1} , and $R(V)_{\text{M.I.S.}}$ is the mean intergalaxy spacing. The κ_{3D} parameters are calculated using one-dimensional velocity dispersions obtained by scaling the true 3D velocity dispersions assuming isotropy (i.e. no strongly radial/tangential orbits for galaxies in mock groups). We define the κ parameters as before, except that we use full 3D information to define the half light, virial radius, and velocity dispersion. The distribution of the resulting groups in κ -space is shown in Figure 16b.

The optimal linking in redshift space is defined as that which produces median group

velocity dispersions and group memberships which best match those formed from grouping in real space in the mock-sky catalog. This optimal redshift linkage, $V_5 = 350$ km/sec for $D_0 = 0.36$, was determined in NKP94 and fortuitously agrees with that used earlier on the CfA1 data to generate the N93 groups catalog used here. The virial-to-true mass ratios of simulated groups selected for the mock-sky catalog with the N93 link criteria have large scatter, but show a median quite close to 1 (NKP97). However, $\sim 20 - 25\%$ of the simulated 3-member groups have such large virial-to-true mass ratios that they are likely chance groupings. This suggests that most CfA1 groups are likely bound, but with some contamination from unbound groups at the 3-member level. There is also confirming evidence from X-ray studies of galaxy groups that at least the E-dominated groups are bound systems, even with as few as 2 giant galaxies (cf. Mulchaey et al. 1996).

As in all of our plots, selection effects will skew the relative density of groups across κ -space. In particular, we preferentially select richer groups both because they can be seen at greater distance and because massive potentials with few galaxies will tend to be missed since their large velocity dispersions will mimic low density in redshift space.

B.2. Results

Figure 16a shows the κ -space distribution for these CHDM₂ groups identified in redshift space using the N93 linking. The distribution of the 3D selected simulation groups in κ -space is shown in Figure 16b. Comparing Figure 16a with Figure 16b, we find that properties change little in going from real to redshift space, so that the fundamental features of the kappa space distributions of observed groups, which of necessity must be identified in redshift space, should be reliable. We find shifts, in the sense redshift-space to real-space, of only 0.3 in κ_1 , -0.2 in κ_2 , and 0.3 in κ_3 . There is one important difference between redshift-selected groups and with real-space selected groups, however. As the simulated volume is small there is a paucity of rich dense clusters in the simulation. In comparing these figures, we've chosen not to focus on individual κ shifts for each group, since not all groups have both redshift-space and real-space counterparts. Some groups break into two, or merge, or members drop out, or new members appear.

We next note that, as in the CfA1 data, there is somewhat of a tendency for the richer groups to show a flatter fundamental plane than poor groups. At least some of this tendency is due to correlated noise. Note that the (noisy) virial mass appears in the numerator of both κ_1 and κ_3 . From Equations 1 and 3, we see that perfectly random masses would yield a “fundamental plane” with slope $\sqrt{2/3} = 0.82$. Since this is steeper than observed, it's not surprising that more poorly sampled and hence noisier groups would show

a steeper FP. However, the fact that the slope is little changed for 3D groups shows that most of slope of their FP is real.

We also find a tendency for the grouping algorithm to miss some valid members on the tail of the redshift distribution for distant massive groups, while including spurious infalling outliers along the line of sight. This latter effect has the tendency to artificially concentrate the group, and thus lower the virial radius and mass. High velocity dispersion systems are more common at high distance. If too many members on the tail of the redshift distribution miss the magnitude cut, they can break the redshift link and miss inclusion. Indeed, the algorithm was tuned to best select average groups and appears to systematically underestimate the dispersion of massive clusters. This may lead to the cutoff in M/L for rich clusters that is somewhat sharper than for the poorer, lower velocity dispersion groups. Of the 5 Abell clusters in N93 which have Struble & Rood (1991) velocity dispersions, the N93 dispersions average 30% smaller ($\Delta \log \sigma = -0.167$). Some part of this effect may also arise from subclustering within clusters.

Finally, we note the striking similarity between the observed (Figure 9) and simulated distributions of groups in κ -space. To some extent, this may reflect the careful choice of simulation and mock-sky constructions. On the other hand, is it possible that the distributions are primarily determined by the gravitation of the dark matter and our simple luminosity assignment method is not far off. If so, the simulations may capture most of the essence of the problem and, if correcting for overmerging leaves κ -space relatively unchanged, the agreement between CHDM and observations may then be significant. In any case, we found that the population differences between rich and poor simulation groups was only a minor factor; richer clusters have galaxies with luminosities only 20 – 30% below those of poorer clusters.

The main cause for the M/L vs. M trend is that there are simply fewer galaxies per unit mass in richer groups. This is seen by calculating $d \log N / d \log M$, where N is the number of visible group members at an arbitrary, but constant distance, and M is the group virial mass. We find $d \log N / d \log M = 0.57, 0.50$ and 0.68 for the redshift space, real space, and breakup versions, respectively. While a more appropriate break-up prescription may well produce more galaxies (NKP97), this hypothetical break-up scheme would have to be quite extreme to make $d \log N / d \log M = 1$.

REFERENCES

Aaronson, M. & Mould, J. R. 1986, ApJ, 265, 1

- Ashman, K. M. & Zepf, S. E. 1992, *ApJ*, 384, 50
- Bardeen, J. M., Bond, J. R., Kaiser, N., & Szalay, A. S. 1986, *ApJ*, 304, 15
- Barnes, J., & Efstathiou, G. 1987, *ApJ*, 319, 575
- Bender, R. 1988, *A&A*, 193, L7
- Bender, R., Burstein, D., & Faber, S.M. 1992, *ApJ*, 399, 462 (B²F1)
- Bender, R., Burstein, D., & Faber, S.M. 1993a, *ApJ*, 411, 153 (B²F2)
- Bender, R., Burstein, D., & Faber, S.M. 1993b, in *Structure, Dynamics and Chemical Evolution of Early-Type Galaxies*, ed. I.J. Danziger, W.W. Zeilinger & K. Kj ar, (ESO: Garching), 31
- Bender, R., Burstein, D., & Faber, S.M. 1995, in *Panchromatic View of Galaxies: Their Evolutionary Puzzle*, eds. G. Hensler et al., (Gif sur Yvettes: Editions Fronti eres), 99
- Binney, J. & Tremaine, S. 1987, *Galactic Dynamics*, (Princeton: Princeton University Press)
- Blumenthal, G. R., Faber, S. M., Primack, J.R. & Rees, M. J. 1984, *Nature* 311, 517 (BFPR)
- Bothun, G.,D., Schombert, J.,M., Impey, C.,D., & Schneider, S.,E. 1990, *ApJ*, 360, 427
- Burstein, D. 1982, *ApJ*, 253, 539 & unpublished
- Burstein, D., Bender, R., Faber, S.,M. & Nolthenius, R. 1995, *Astro Lett & Comm*, 31, 95 (B²FN)
- Burstein, D. & Heiles, C. 1978, *ApJ*, 220, 40
- Burstein, D. & Heiles, C. 1982, *AJ*, 87, 1162
- Cen, R. & Ostriker, J. 1994, *ApJ*, 431, 451
- Dalcanton, J.J., 1997, Ph. D. Thesis, Univ Cal Santa Cruz
- Davis, M., Huchra, J., Latham, D.,W., & Tonry, J. 1982, *ApJ*, 253, 423
- Davies, R. L., Efstathiou, G., Fall, S. M., Illingworth, G. & Schechter, P. 1983, *ApJ*, 266, 41
- Davies, R. L., Burstein, D., Dressler, A., Faber., S. M., Lynden-Bell, D., Terlevich, R. J., & Wegner, G. 1987, *ApJS*, 64, 581
- Dekel, A. & Silk, J. 1986, *ApJ*, 303, 39
- de Vaucouleurs, G. & de Vaucouleurs, A., 1964, *Reference Catalog of Bright Galaxies* (Austin: University of Texas) (RC1)

- de Vaucouleurs, G., de Vaucouleurs, A., Corwin, H. C. G., Jr., Buta, R. J., Paturel, G. & Fouqué, P. 1991, *Third Reference Catalog of Bright Galaxies* (New York: Springer-Verlag) (RC3)
- Djorgovski, S. 1995, *ApJL*, 438, 29
- Djorgovski, S. & Davis, M. 1987, *ApJ*, 313, 59
- Djorgovski, S. & Meylan, G. 1993, in *Structure and Dynamics of Globular Clusters*, ASP Conf Series 50, eds. S. G. Djorgovski & G. Meylan (San Francisco: ASP), p. 325
- Dressler, A., Faber, S. M., Burstein, D., Davies, R. L., Lynden-Bell, D., Terlevich, R. and Wegner, G. 1987, *ApJL*, 313, 37
- Dressler, A. 1980, *ApJ*, 236, 351
- Dressler, A. 1988, *ApJ* 329, 519
- Faber, S. M. 1982a, in *Astrophysical Cosmology: Proc Study Week on Cosmology and Fundamental Physics*, ed. H. A. Brück, G. V. Coyne & M. S. Longair (Vatican: Pontifical Sci Acad), 191
- Faber, S. M. 1982b, in *Astrophysical Cosmology: Proc Study Week on Cosmology and Fundamental Physics*, ed. H. A. Brück, G. V. Coyne & M. S. Longair, (Vatican: Pontifical Sci Acad), 219
- Faber, S., M. 1983, in *Large-Scale Structure of the universe, Cosmology, and Fundamental Physics*, eds. G. Setti and L. van Hove (Geneva: CERN), 187
- Faber, S. M. & Burstein, D., 1988, in *Large-scale Motions in the universe*, eds. V. C. Rubin and G. V. Coyne, (Princeton: Princeton U. Press), 115
- Faber, S.M., Dressler, A., Davies, R. L., Burstein, D., Lynden-Bell, D. and Terlevich, R., & Wegner, G. 1987, in *Nearly Normal Galaxies: From the Planck Time to the Present*, ed. S. M. Faber (New York: Springer), 175
- Faber, S. M. & Jackson, R. E. 1976, *ApJ*, 204, 668
- Faber, S. M., Wegner, G., Burstein, D., Davies, R. L., Dressler, A., Lynden-Bell, D. and Terlevich, R. 1989, *ApJS*, 69, 763
- Faber, S. M., et al. 1997, *ApJ*, submitted
- Fabian, A.C. 1994, *ARAA*, 32, 277
- Fall, M. & Efstathiou, G. 1980, *MNRAS* 193, 189
- Fall, S. M., & Rees, M. J. 1985, *ApJ*, 298, 18
- Freeman, K. C. 1970, *ApJ* 160, 811

- Gallego, J., Zamorano, J., Rego, M., Alonso, O. Vitores,, A. G. 1996, *A&AS*, 120, 323.
- Geller, M. J., & Huchra, J. P. 1983, *ApJS*, 52, 61
- Gnedin, O. Y., & Ostriker, J. P. 1997, *ApJ*, 474, 223
- Gott, J. R., and Rees, M. J. 1975, *A&A*, 15, 235.
- Holtzman, J. A., et al. 1992, *AJ*, 103, 691
- Impey, C. & Bothun, G. D. 1989, *ApJ*, 341, 89
- Jaffe, W. 1983, *MNRAS* 202, 995
- Jørgensen, I., Franx, M., & Kjaergaard, P. 1996, *MNRAS*, 280, 167
- Katz, N. & White, S.D.M. 1993, *ApJ*, 412, 455
- Kauffmann, G., White, S. D. M., & Guiderdoni, B. 1993, *MNRAS* 261, 921
- King, I. R. 1966, *AJ*, 71, 64
- Klypin, A.A., Nolthenius, R., & Primack, J.R. 1997, *ApJ* 474, 533
- Klypin, A.A., Holtzman, J.A., Primack, J.R., & Regos, E. 1993, *ApJ*, 416, 1
- Koo, D.C., Bershadsky, M.A., Wirth, G.D., Stanford, S.A., & Majewski, S.R. 1994, *ApJL*, 427, L9
- Kormendy, J. 1988, in *Origin, Structure and Evolution of Galaxies*, IAU Symp 127, ed. L. Z. Fang, (Singapore: World Scientific), 252
- Kormendy, J. 1989, *ApJ*, 342, L63
- Kormendy, J. & Bender, R. 1996, *ApJL*, 464, L119
- Krumm, N. & Burstein, D. 1984 *AJ*, 89, 1319
- Lin, D. & Faber, S.M. 1983, *ApJL*, 266, L21
- McGaugh, S.S. 1996, *MNRAS*, 280, 337
- Tremblay, B. & Merritt, D. 1996, *AJ*, 111, 2243
- Moore, B., Katz, N., Lake, G., Dressler, A., and Oemler, A. 1996, *Nature*, 379, 6566.
- Mulchaey, J.S., Davis, D.S. Mushotzky, R.F. & Burstein, D. 1996, *ApJ* 456, 80
- Mushotzky, R. F. 1991, in *After the First Three Minutes*, eds. S. S. Holt, C. L. Bennett & V. Trimble, (New York: AIP), 394
- Nieto, J.-L., Bender, R., Davoust, E. & Prugniel, P. 1990, *A&A* 230, L17
- Nolthenius, R. 1993, *ApJS*, 85, 1
- Nolthenius, R., & White, S. D. M. 1987, *MNRAS*, 225, 505

- Nolthenius, R., Klypin, A. A., & Primack, J. R. 1994, *ApJL* 422, L45 (NKP94)
- Nolthenius, R., Klypin, A. A., & Primack, J. R. 1997, *ApJ*, 480, 43 (NKP97)
- Peebles, P. J. E. 1969, *ApJ*, 155, 393
- Peebles, P. J. E., & Dicke, R. H. 1968, *ApJ*, 154, 891
- Peterson, C. J. 1993, in *Structure and Dynamics of Globular Clusters*, ASP Conf Series 50, eds. S. G. Djorgovski & G. Meylan (San Francisco: ASP), 337
- Postman, M., & Geller, M. 1984, *ApJ*, 281, 95
- Pryor, C. & Meylan, G. 1993, in *Structure and Dynamics of Globular Clusters*, ASP Conf Series 50, ed. S. G. Djorgovski & G. Meylan (San Francisco: ASP), 357
- Rees, M. J., and Ostriker, J. P. 1977, *MNRAS*, 179, 541
- Renzini, A. 1994, in *Galaxy Formation*, International School of Physics “E. Fermi” Course CXXII, eds. J. Silk & N. Vittorio (Amsterdam: North Holland), 303
- Rosenblatt, E. I., Faber, S. M., & Blumenthal, G. 1988, *ApJ*, 330, 191.
- Rubin, V. C., Burstein, D., Ford, W. K., and Thonnard, N. 1985, *ApJ*, 289, 91
- Saglia, R. P., Bender, R. & Dressler, A. 1992 *A&A*, 275, 79
- Salzer J.J., MacAlpine, G.M., & Boroson, T.A. 1989, *ApJS*, 70, 447
- Schaeffer, R., Maurogordato, S., Cappi, A., & Bernardeau, F. 1993, *MNRAS*, 263, L21
- Schechter, P. 1976, *ApJ*, 203, 297
- Searle, L. & Zinn, R. 1978, *ApJ*, 225, 357
- Struble, M. F. & Rood, H.J. 1991, *ApJS*, 77, 363
- Tinsley, B. M. 1981, *MNRAS*, 194, 63
- Toomre, A. 1964, 139, 1217
- Toomre, A. 1981, in *The Structure and Evolution of Normal Galaxies*, eds. M. S. Longair & D. Lynden-Bell (Cambridge: Cambridge University Press), p. 111
- Trager, S. C., Djorgovski, G. & King, I. R. 1993, in *Structure and Dynamics of Globular Clusters*, ASP Conf Series 50, ed. S. G. Djorgovski & G. Meylan (San Francisco: ASP), 347
- Tully, R. B. & Fisher, J. R. 1977, *A&A*, 54, 661
- Verheyen, M. 1997, Ph.D. Thesis, University of Groningen
- Whitmore, B. C. & Kirshner, R. P. 1981, *ApJ*, 250, 43

Worthey, G. 1994, ApJS, 95, 107

FIGURE CAPTIONS

Figure 1 The κ parameters for spiral galaxies in the Virgo cluster, and elliptical galaxies in Virgo and in the Coma cluster, plotted in a three-dimensional fold-out of κ -space. Symbols as given in the legend, used only for this figure. Dark lines represent $\pm 30\%$ distance errors. The dashed line in the κ_1 - κ_2 plane is the zone of exclusion line (ZOE) discussed in the text, $\kappa_1 + \kappa_2 = 8$. The solid line in the κ_1 - κ_3 plane is the gE fundamental plane. The dashed and solid lines in the κ_2 - κ_3 are the projection of the fundamental plane in this projection. Note how, in absence of distance errors, spiral galaxies and elliptical galaxies occupy similar regions in κ -space.

Figure 2 κ parameters for dynamically hot galaxies (DHGs), plotted in the same 3D fold-out manner as in Figure 1. The plotting symbols here are chosen to highlight the positions of isotropic DHGs (open squares and diamonds) versus anisotropic DHGs (closed squares and diamonds) in κ -space, as well as to separate giant DHGs from dwarf DHGs. These data come from B²F1. Small open squares are galaxies from the 7Samurai data set (Faber et al. 1989) with no isotropy measurements.

Figure 3 κ parameters for Sa+Sab galaxies (broad crosses) and Sb galaxies (open hexagons) plotted in the same 3D fold-out manner as in Figure 1. These early-type spirals are now farther from the ZOE in the κ_1 - κ_2 plane, and lie below the DHG fundamental plane in κ_1 - κ_3 . The two galaxies that lie just on the ZOE are NGC 669 and the well-known bulge-dominated Sa galaxy NGC 4594.

Figure 4 κ parameters for Sbc galaxies (closed triangles) and Sc galaxies (open circles) plotted in the same 3D fold-out manner as in Figure 1. These later-type spirals have now marched even further from the ZOE.

Figure 5 κ parameters for Scd galaxies (open pentagons), Sd galaxies (stars), Irregular galaxies (dark crosses) and the two very large spiral galaxies Malin 1 and Malin 2 (large crosses), plotted in the same 3D fold-out manner as in Figure 1. These very late-type spirals occupy roughly the same region as the dwarf DHGs (dE's and dSph's), suggesting that the latter may have originated from the former via gas loss. Two of the lowest mass Irr galaxies in this sample (A 22044-1 = DDO 210 and Leo A = DDO 69) lie intermediate in κ properties between the dE and dSph galaxies.

Figure 6. Histograms of the distance of galaxies from the ZOE defined by DHGs in the κ_1 - κ_2 plane. The residuals are defined as $\delta_{2,1} = \kappa_1 + \kappa_2 - 8$. The diagram summarizes and quantifies the march of Hubble types away from the ZOE in the previous figures.

Figure 7 Histograms of the distance of galaxies from the DHG fundamental plane. The

residuals are defined as $\delta_{3:1} = \kappa_3 - 0.15\kappa_3 - 0.36$. Bin size is 0.05 dex. This diagram reflects conclusions from Figures 2–5: Sa–Sc galaxies define a fundamental plane that is basically parallel to that for DHGs but offset by -0.2 dex to lower κ_3 values. Hubble types Scd–Irr define yet a third fundamental plane with a different tilt and showing negligible slope in $\kappa_1 - \kappa_3$.

Figure 8 The B-band Tully-Fisher relation for the spiral and irregular galaxies in our sample. Symbols for the different Hubble types are as in Figures 3–5. A line of slope -7.5 (which corresponds to $A_C = 3$, Equation 26) is drawn through the data. A line with $A_C = 4$ corresponds to a plane that projects with minimal scatter onto $\kappa_2 - \kappa_3$. Comparison of points here with $\kappa_2 - \kappa_3$ in Figures 3–5 shows systematic residuals that reflect $A_C = 3$ rather than $A_C = 4$.

Figure 9 κ parameters for galaxy groups and galaxy clusters. Galaxy groups are divided into S-rich (triangles) and E-rich (circles); within each class, groups are separated into those with 10 or more members (closed symbols) or 9 or less (open symbols). Data for 16 rich clusters from Schaeffer et al. are plotted as large closed circles, and data for two very large spiral galaxies Malin 1 and Malin 2 are plotted as large crosses. This 3D diagram samples a different region of κ -space than do Figures 2–5 to accommodate the larger masses, lower surface brightnesses and larger mass-to-light ratios for galaxy groups and clusters.

Figure 10 Histograms of the distance of galaxy groups and galaxy clusters from the DHG fundamental plane. The residuals are the same as in Figure 7, defined as $\delta_{3:1} = \kappa_3 - 0.15\kappa_3 - 0.36$. Globular clusters and DHGs are included for reference. For groups and clusters, mean offset $\delta_{3:1}$ is correlated with both group size and the mean Hubble type of member galaxies, and the distributions are wider for poor groups of all types. These behaviors are consistent with the strong trend of κ_3 vs. κ_1 (M/L vs M) in Figure 9.

Figure 11 The cosmic metaplane. The κ parameters for all of the stellar systems studied in this paper. Symbols for each kind of objects are as in the previous κ diagrams, with the addition of the data for globular clusters, plotted as large closed triangles. At the large scale of this 3D fold-out it is difficult to make out the separate Hubble types for galaxies. Yet, at this scale we can most easily see the overall relationships among the κ parameters for all these stellar systems, which we now define as the cosmic metaplane.

Figure 12 (a) The distribution of all galaxies in our sample (small solid squares) and the distribution of galaxy groups and clusters (open and closed circles) in $\kappa_1 - \kappa_2$. V_1 , V_2 , and V_3 are the three vectors connecting individual E galaxies with E-rich clusters discussed in the text. V_1 undoes the effects of baryonic dissipative infall within dark halos (same as the separate vector labeled “dissipation”). V_2 connects the dark halos of galaxies with

those of E-rich groups along the locus of an $n = -1.8$ power-law density fluctuation spectrum. V_3 is a final correction to the surface brightnesses of clusters owing to their higher hot gas content. Details of all vectors are given in the text. The sum of the three vectors is a fair match to the slope of the ZOE, consistent with the combined predictions of hierarchical clustering/merging and dissipation. (b) A schematic attempt to undo the effects of baryonic dissipation in galaxy halos by sliding galaxies back along the dissipation vector of Figure 12a. The shifted positions show galaxies as they would appear if their stars were redistributed with the same spatial distribution as their dark matter. The recovered, pre-dissipation halos blend smoothly with groups and clusters, showing that the previous separation was due to dissipation. For this shift, a shrinkage in M_e and R_e by a factor of 10 was assumed, with no change in σ_c .

Figure 13 The analogue to Figure 3 in BFPR, plotting baryonic number density versus effective kinetic temperature for all stellar systems. Conversion formulae from κ -parameters to $n_{bary,e}$ and T_e are given in the text. The distribution of galaxies here using real data is fat and horizontal, quite different from the thin, tilted distribution using schematic data in BFPR. The slope of clustering from a power-law density fluctuation spectrum with constant dissipation and $n = -1.8$ is shown.

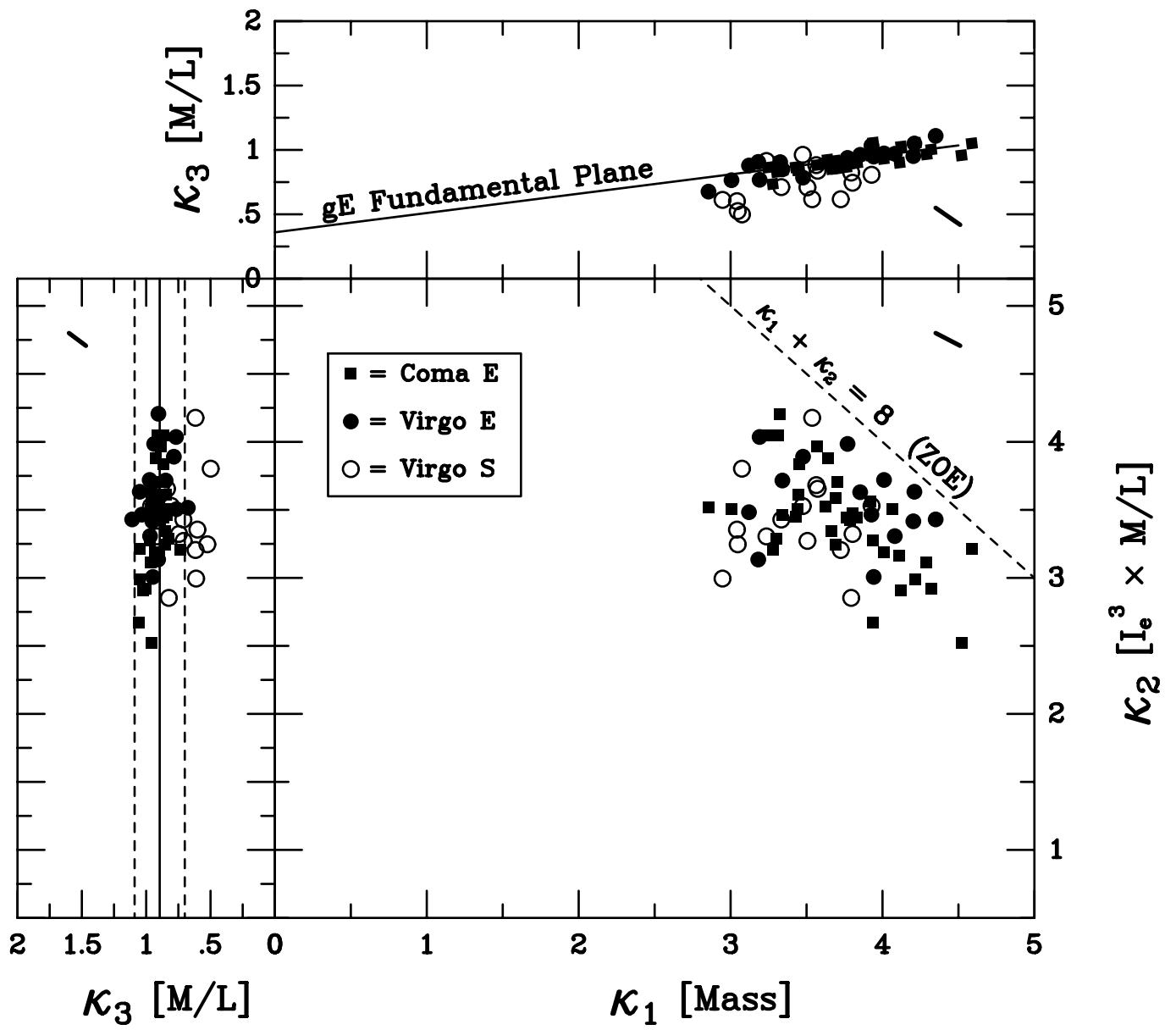
Figure 14 The analogue to Figure 4 in BFPR, in which we now plot M_e (in units of solar masses) versus effective kinetic temperature. The slope of a power-law density fluctuation spectrum with constant dissipation and $n = -1.8$ is shown.

Figure 15 The companion diagram to Figures 13 and 14, plotting a direct analogue to the Tully-Fisher relationship using mass and radius. The slope of a power-law density fluctuation spectrum with constant dissipation and $n = -1.8$ is shown.

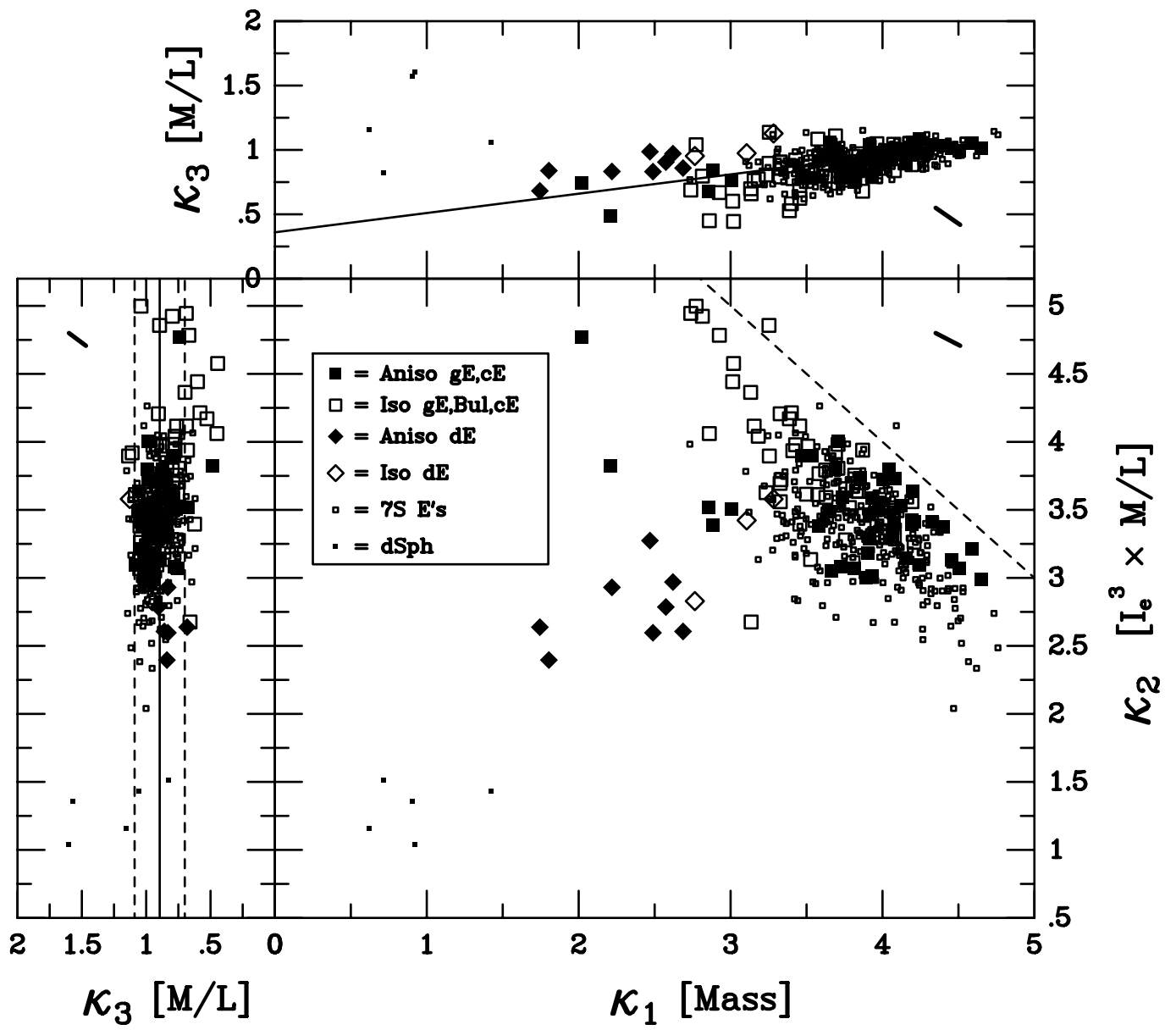
Figure 16 (a) The predicted distribution within κ -space for the CHDM₂ model of Klypin et al. (1993), based on groupings made in redshift space. This simulation mimics the manner in which groups are constructed using real data. The distribution of these mock-groups is a reasonable match to that of real groups. (b) The predicted distribution within κ -space for the CHDM₂ model of Klypin et al. (1993), based on groupings made in distance space (i.e., using fully three dimensional information that is not generally available with real data). It is reassuring that the distribution of these distance-selected mock-groups is quite similar to those both for real groups and for mock-groups selected in redshift space.

Table 2. n - σ Overdensities of Hubble Types

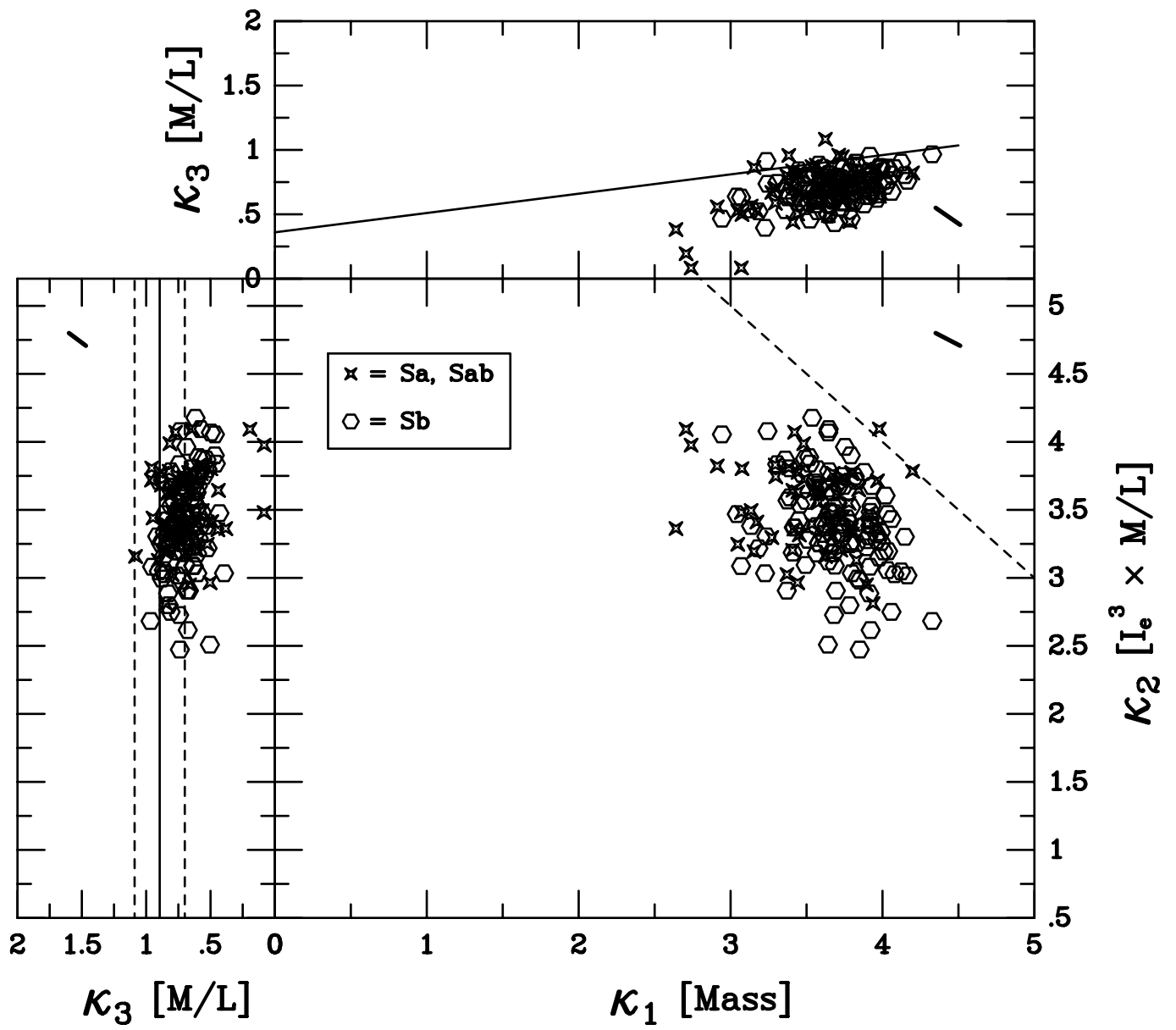
Type	$\Delta\delta_{2:1}$	n - σ (gE \equiv 3)	n - σ (Sc \equiv 1)
gE	0.00	3	1.81
Sa	-0.20	2.48	1.50
Sab,b	-0.21	2.46	1.48
Sbc	-0.36	2.14	1.29
Sc	-0.63	1.66	1
Scd	-1.34	0.85	0.51
Sd	-1.97	0.47	0.28
Irr I	-2.46	0.30	0.18



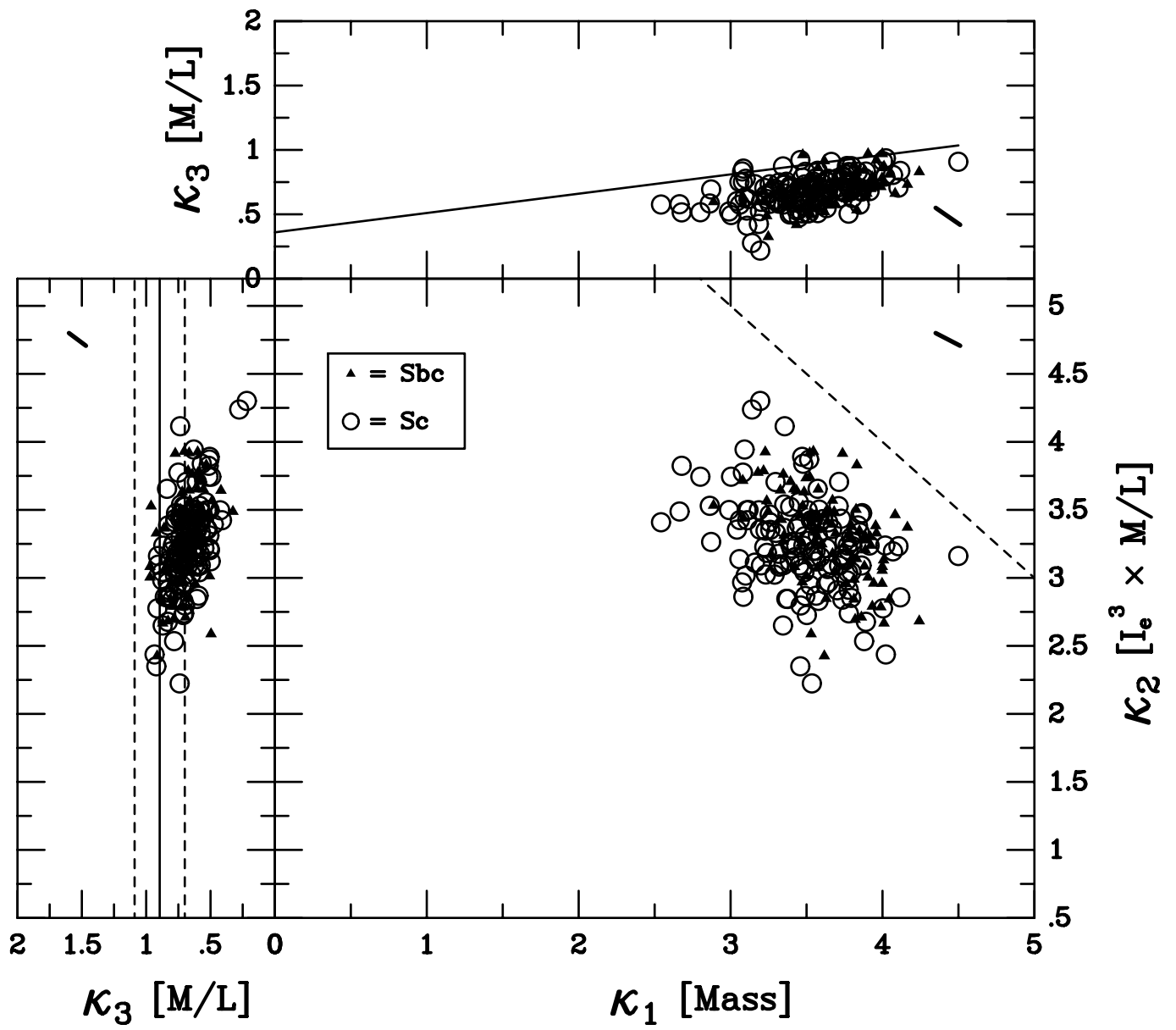
Burstein, Bender,
 Faber, Nolthenius
 1997 AJ Figure 1



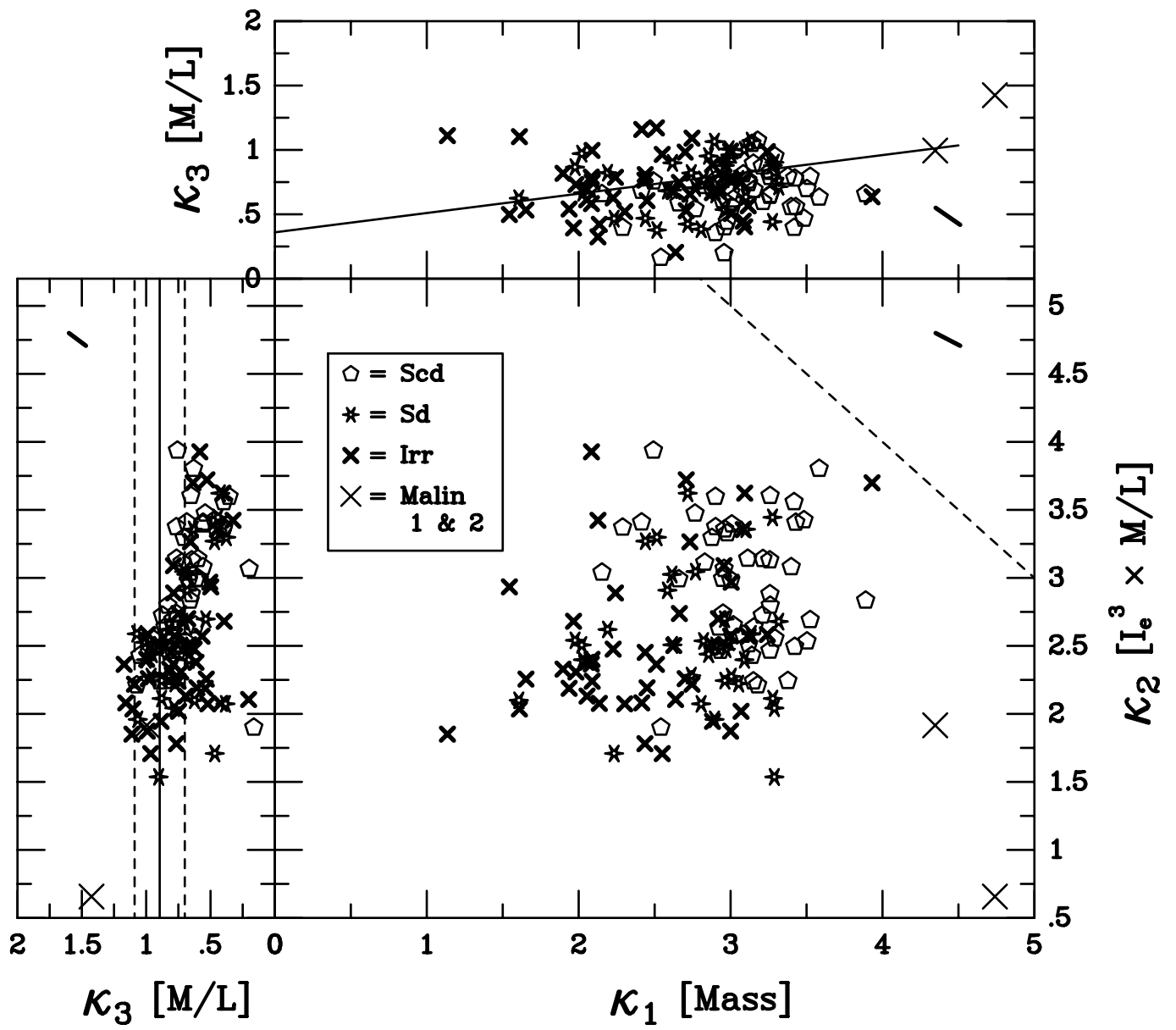
Burstein, Bender,
 Faber, Nolthenius
 1997 AJ Figure 2



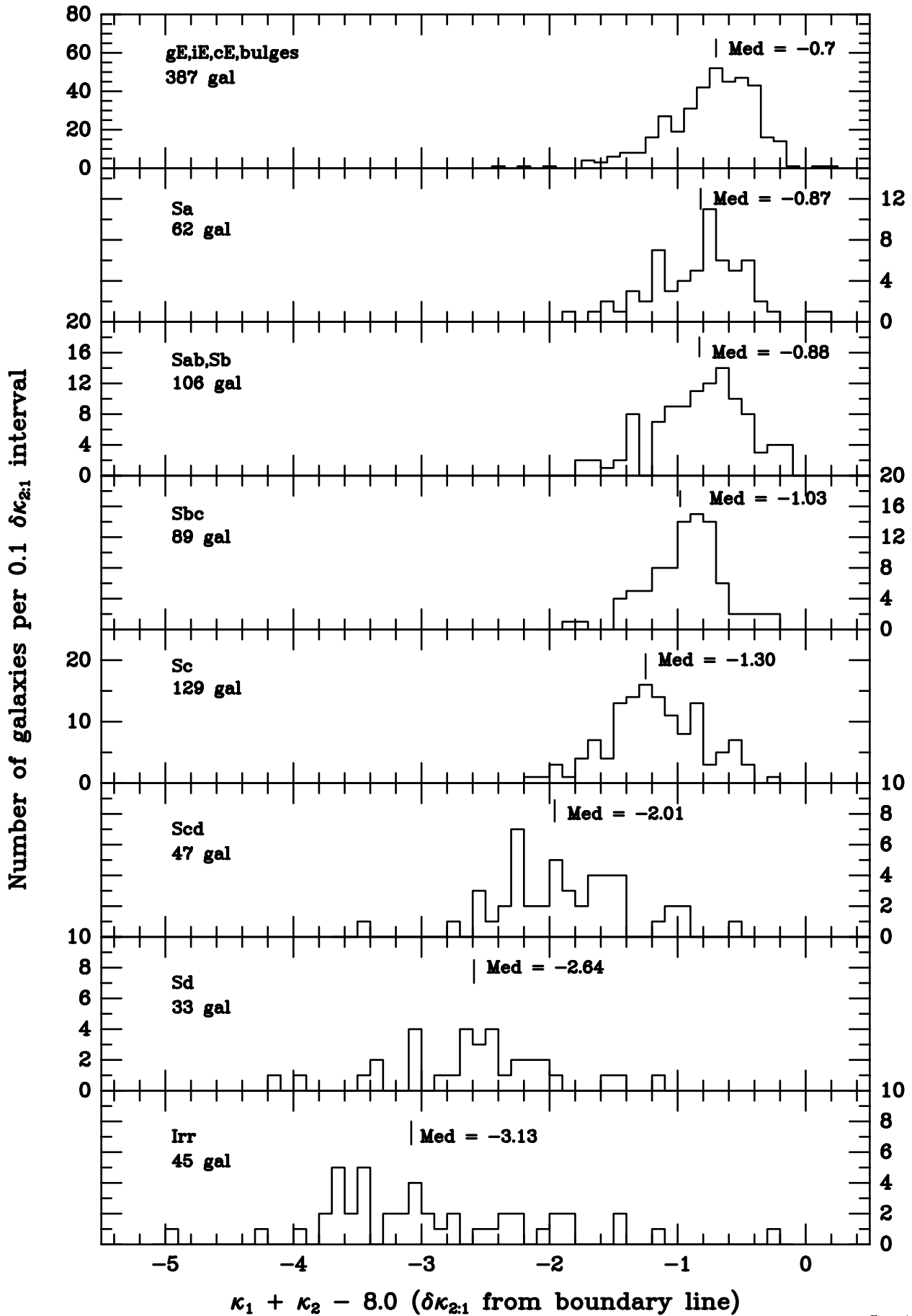
Burstein, Bender,
 Faber, Nolthenius
 1997 AJ Figure 3

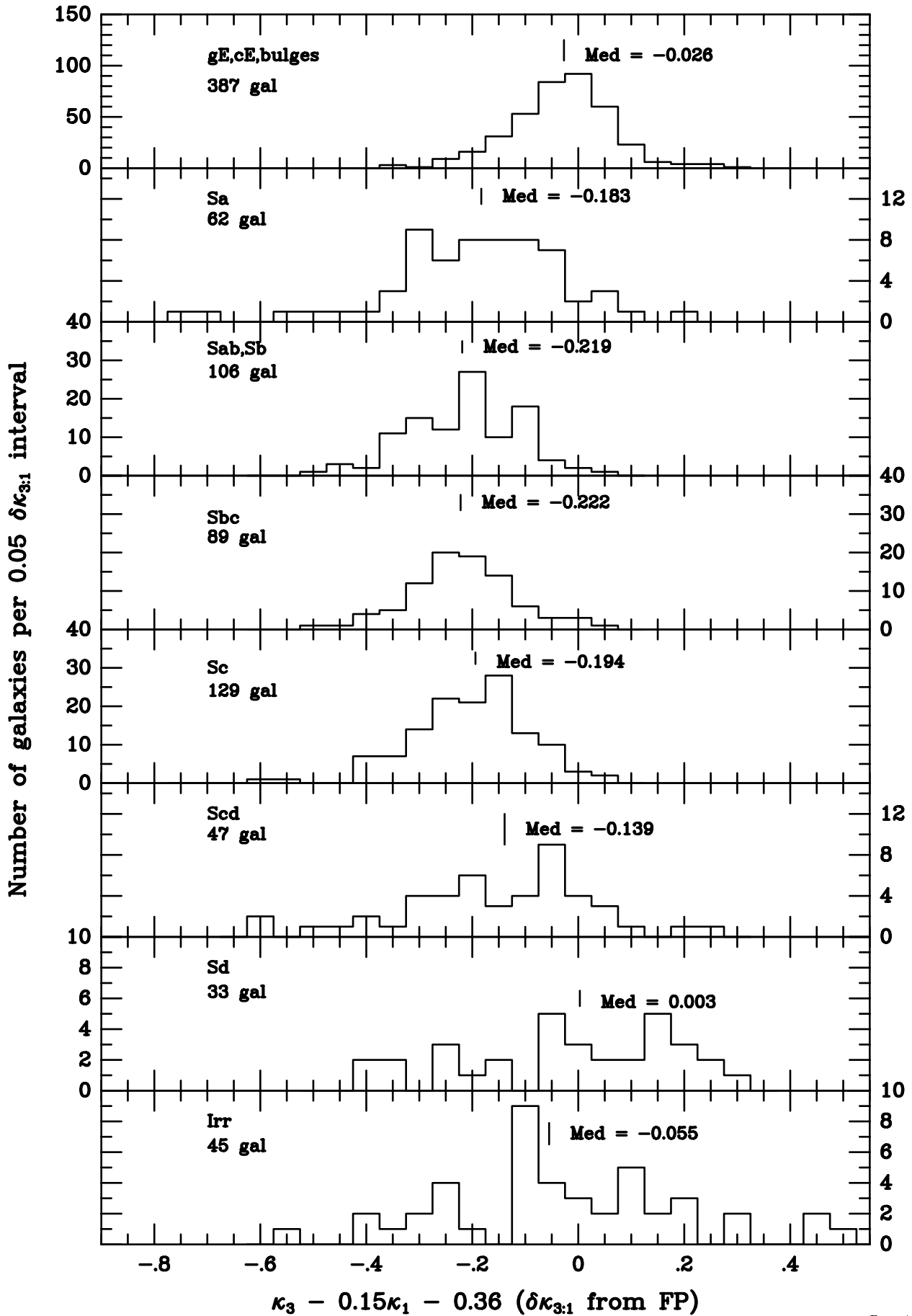


Burstein, Bender,
 Faber, Nolthenius
 1997 AJ Figure 4

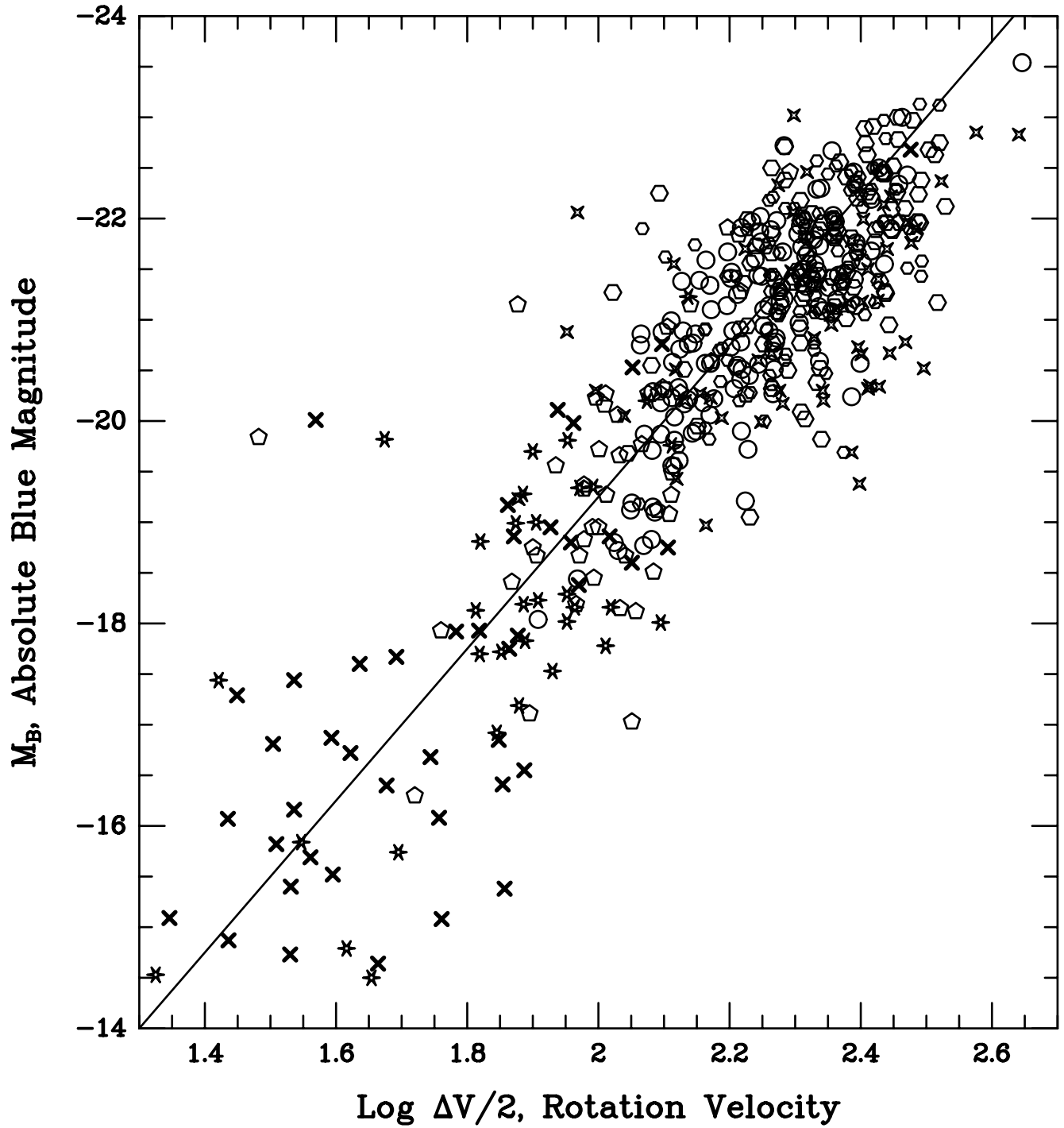


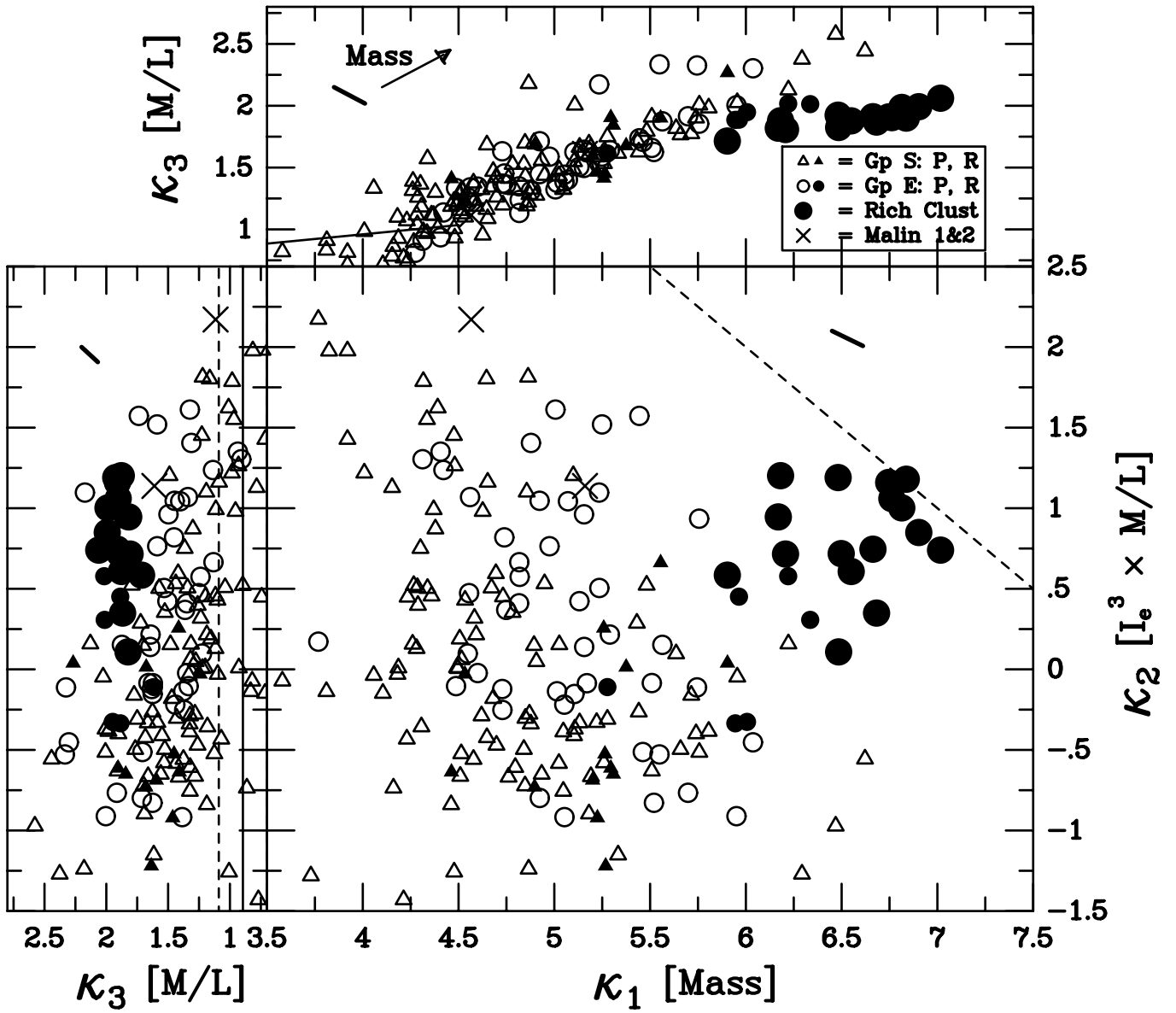
Burstein, Bender,
 Faber, Nolthenius
 1997 AJ Figure 5



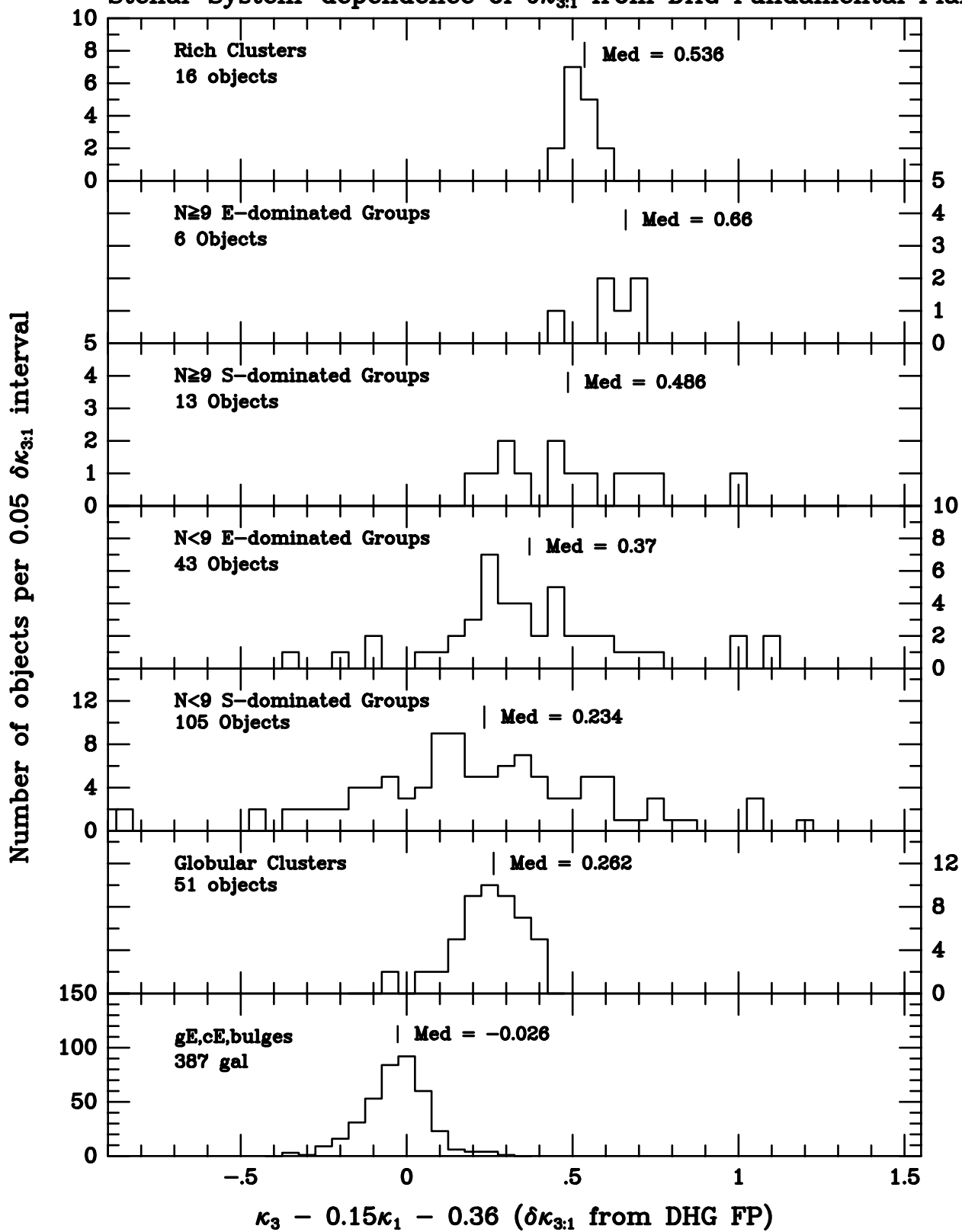


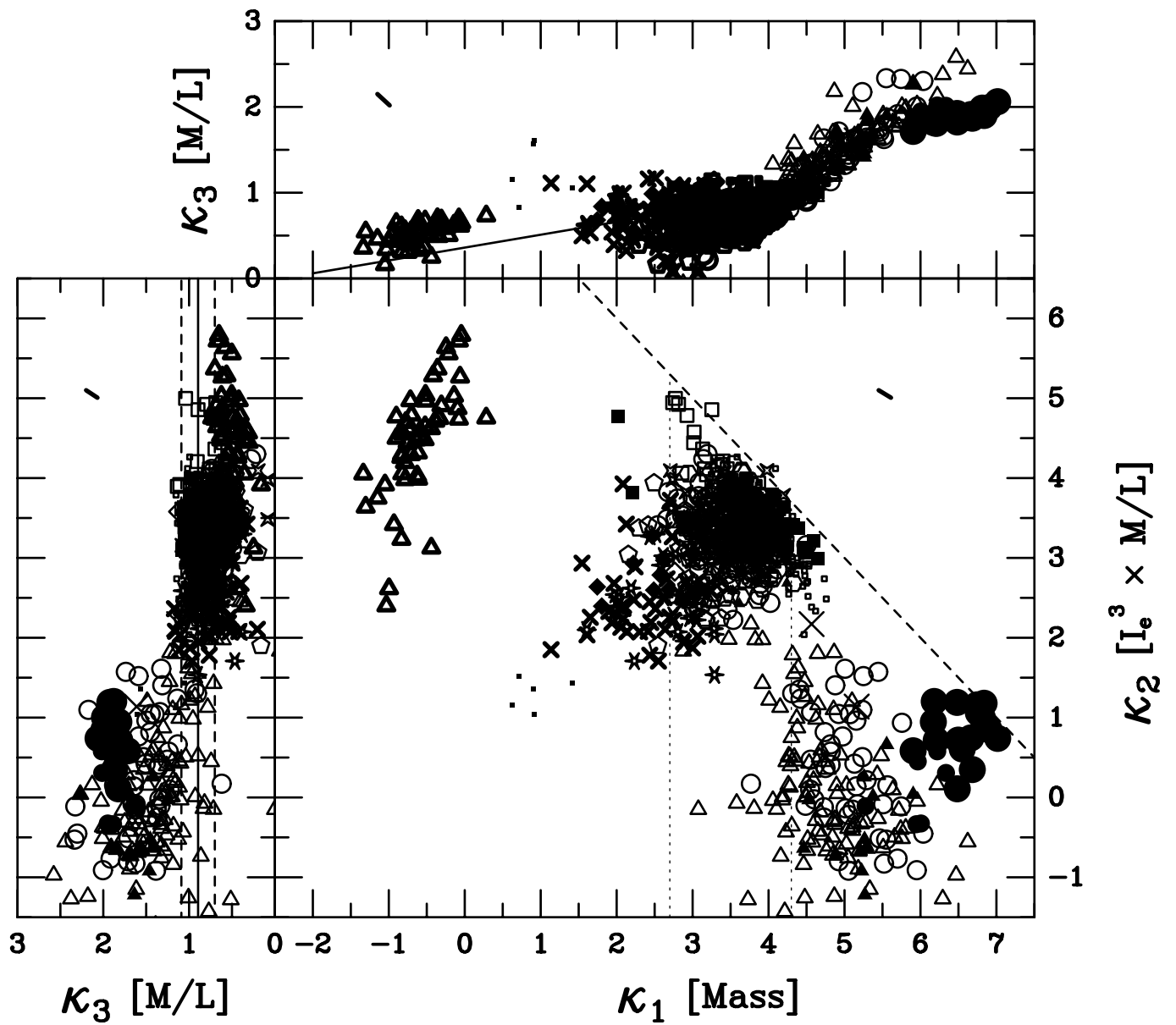
Blue Tully–Fisher Relation for κ -space Galaxies



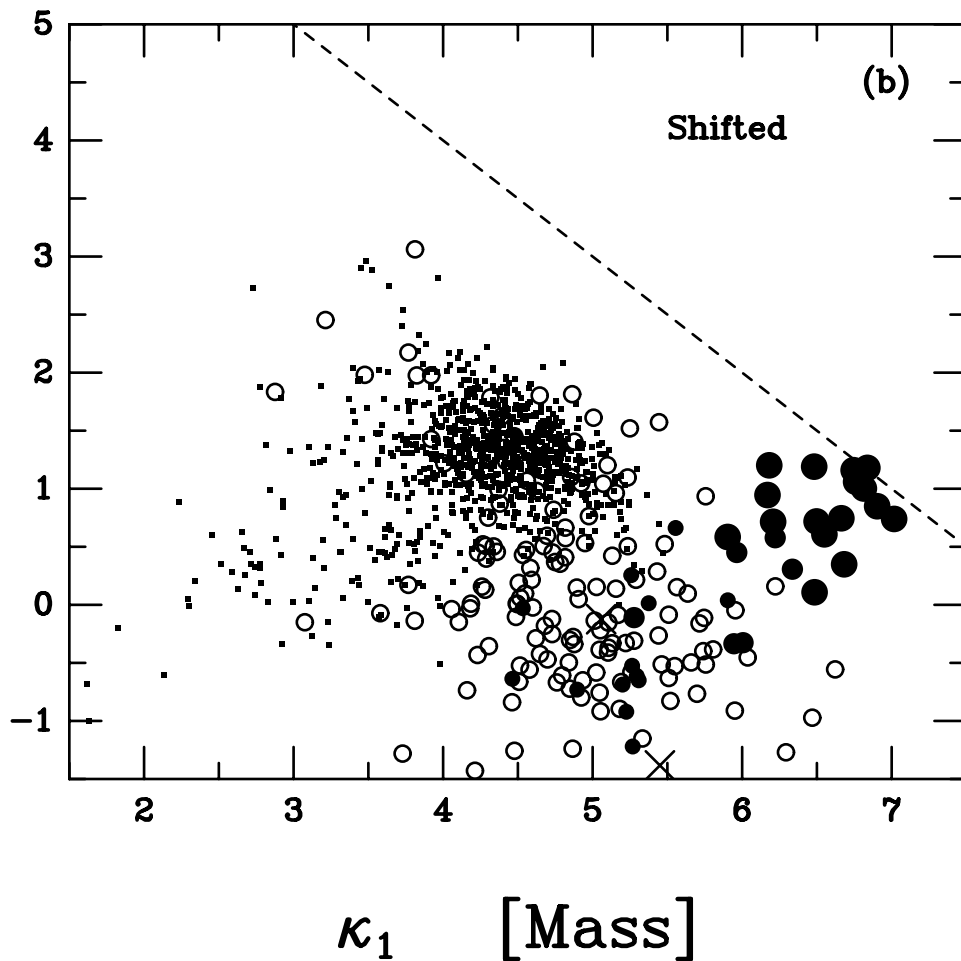
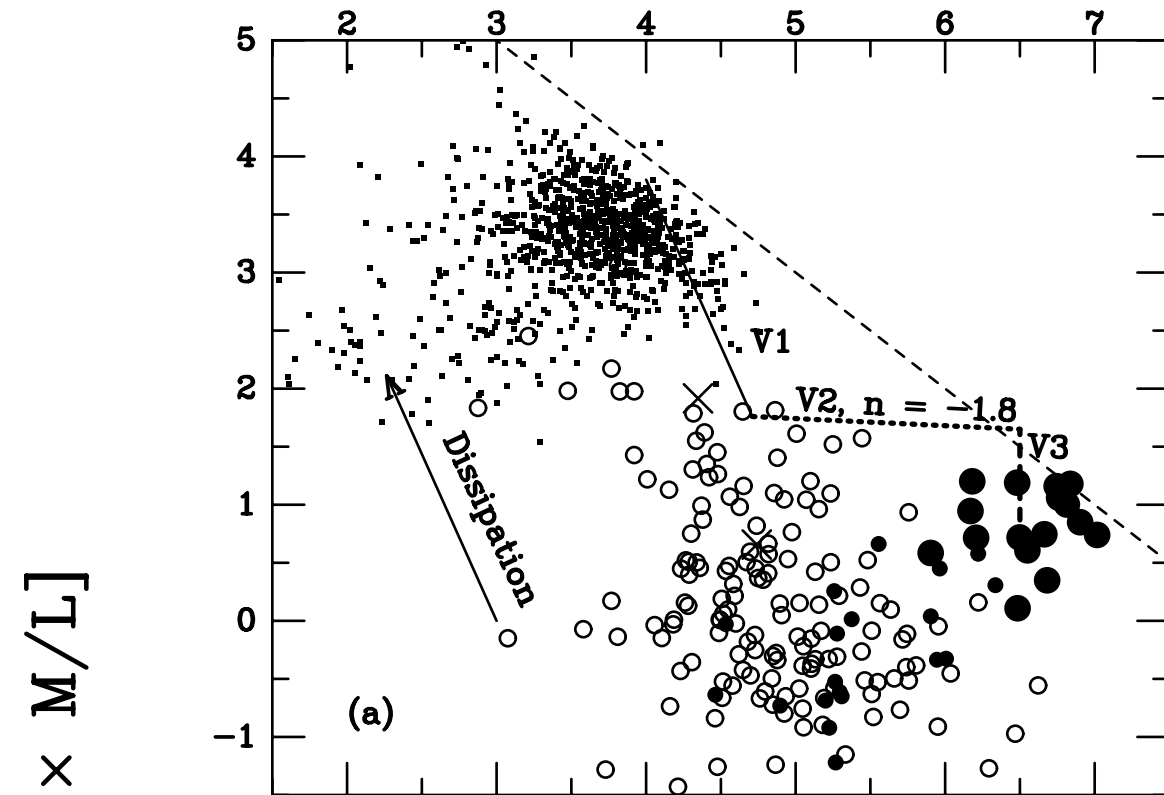


Stellar System-dependence of $\delta\kappa_{3:1}$ from DHG Fundamental Plane

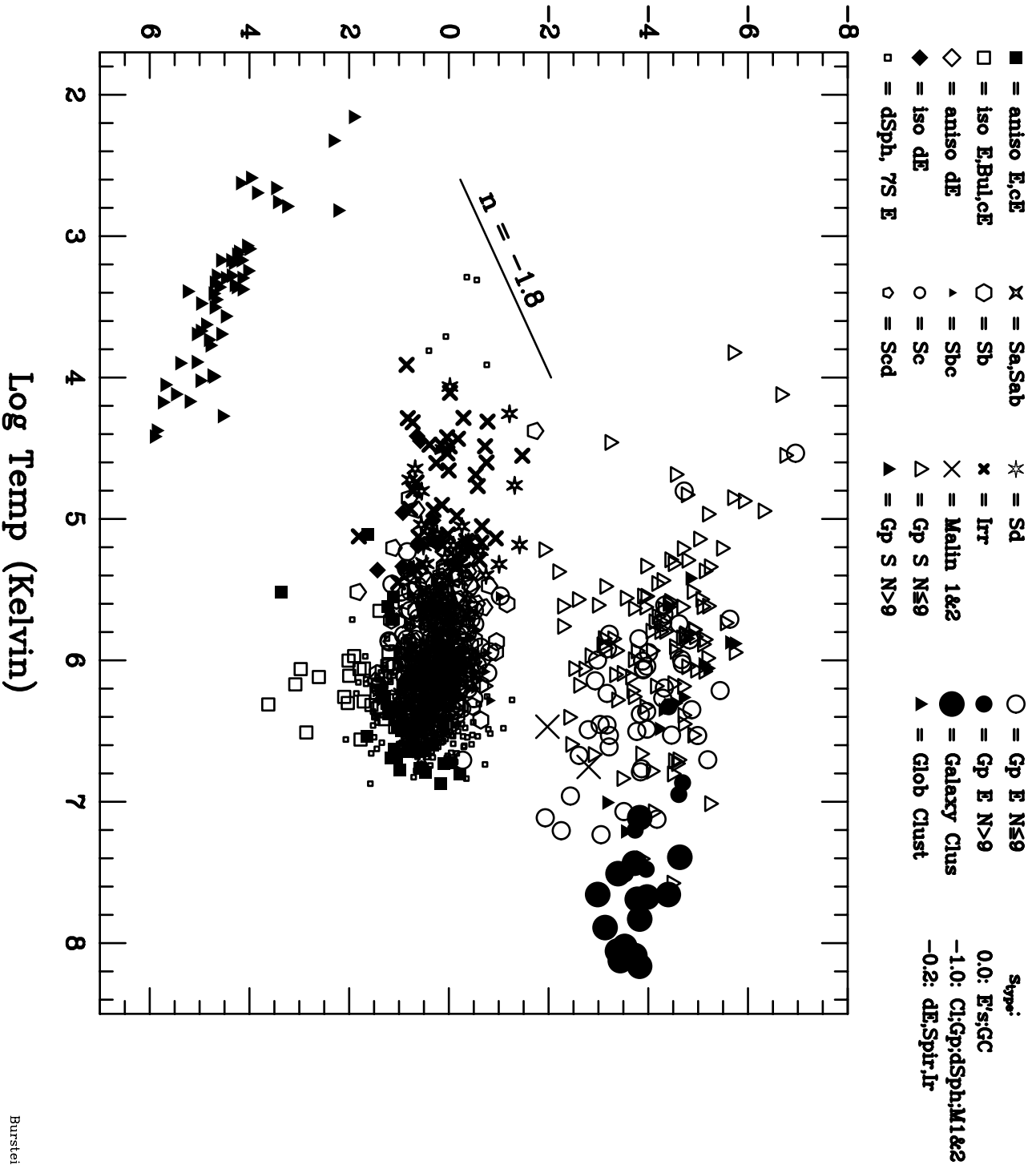


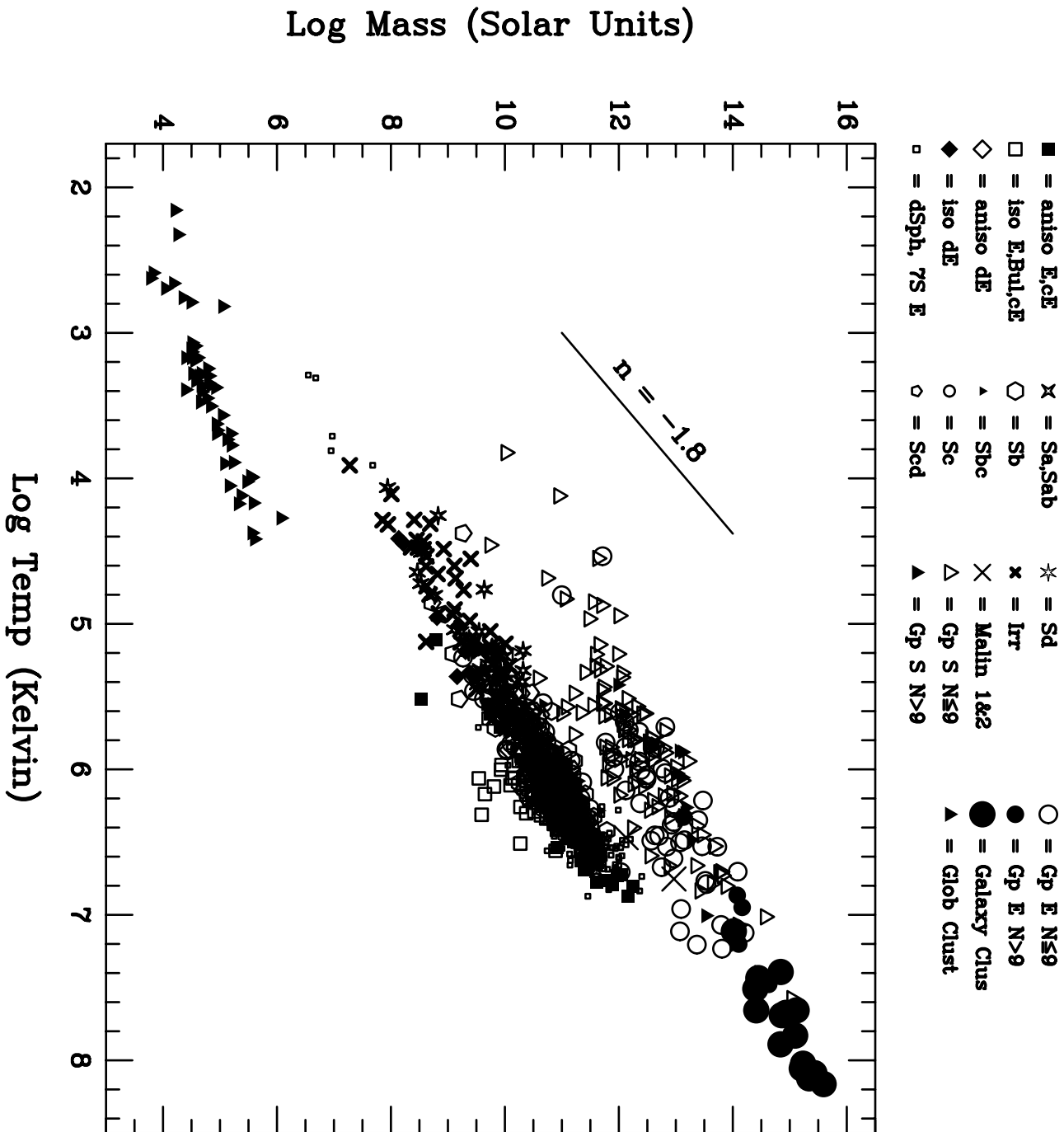


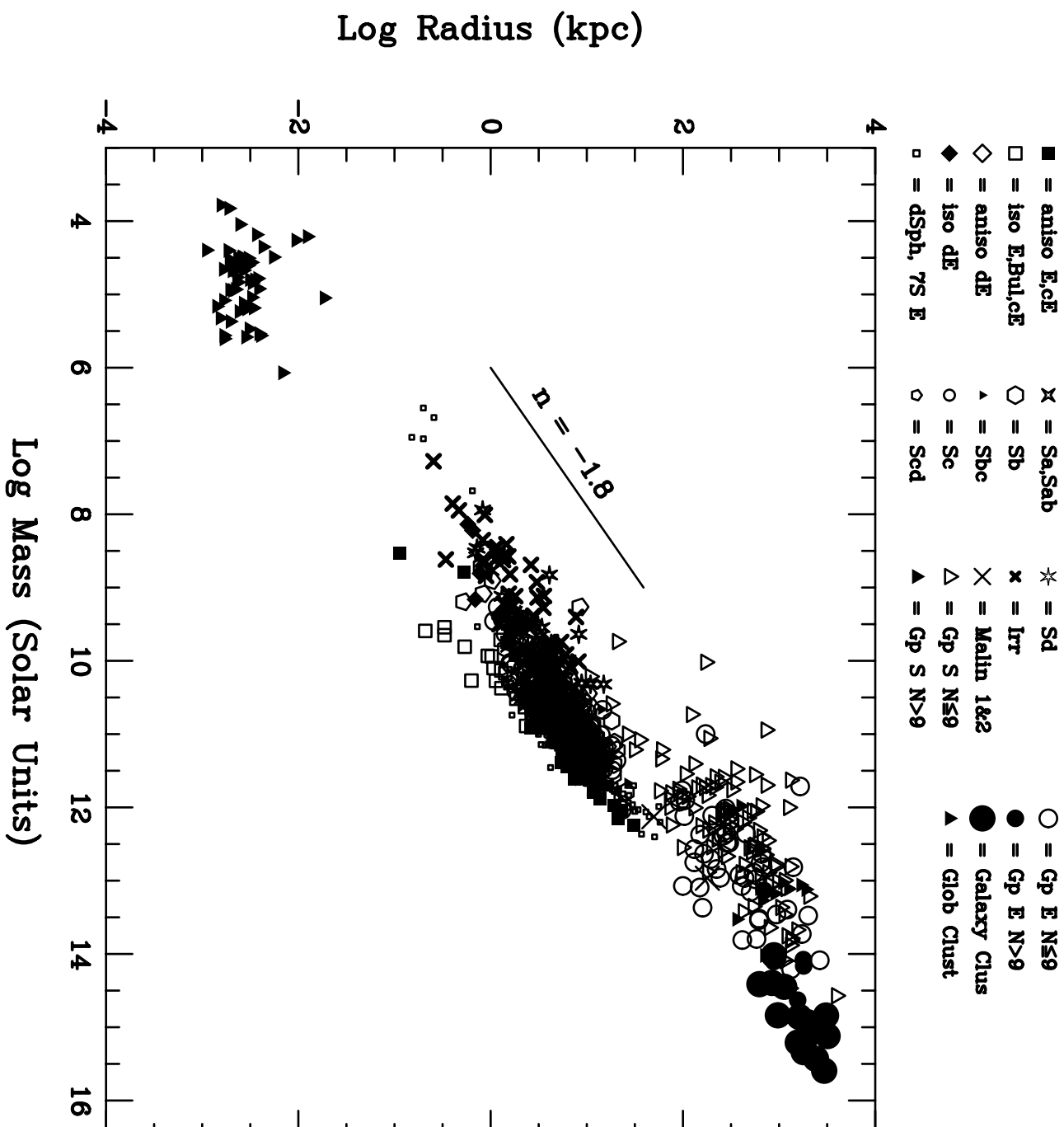
Burstein, Bender,
 Faber, Nolthenius
 1997 AJ Figure 11



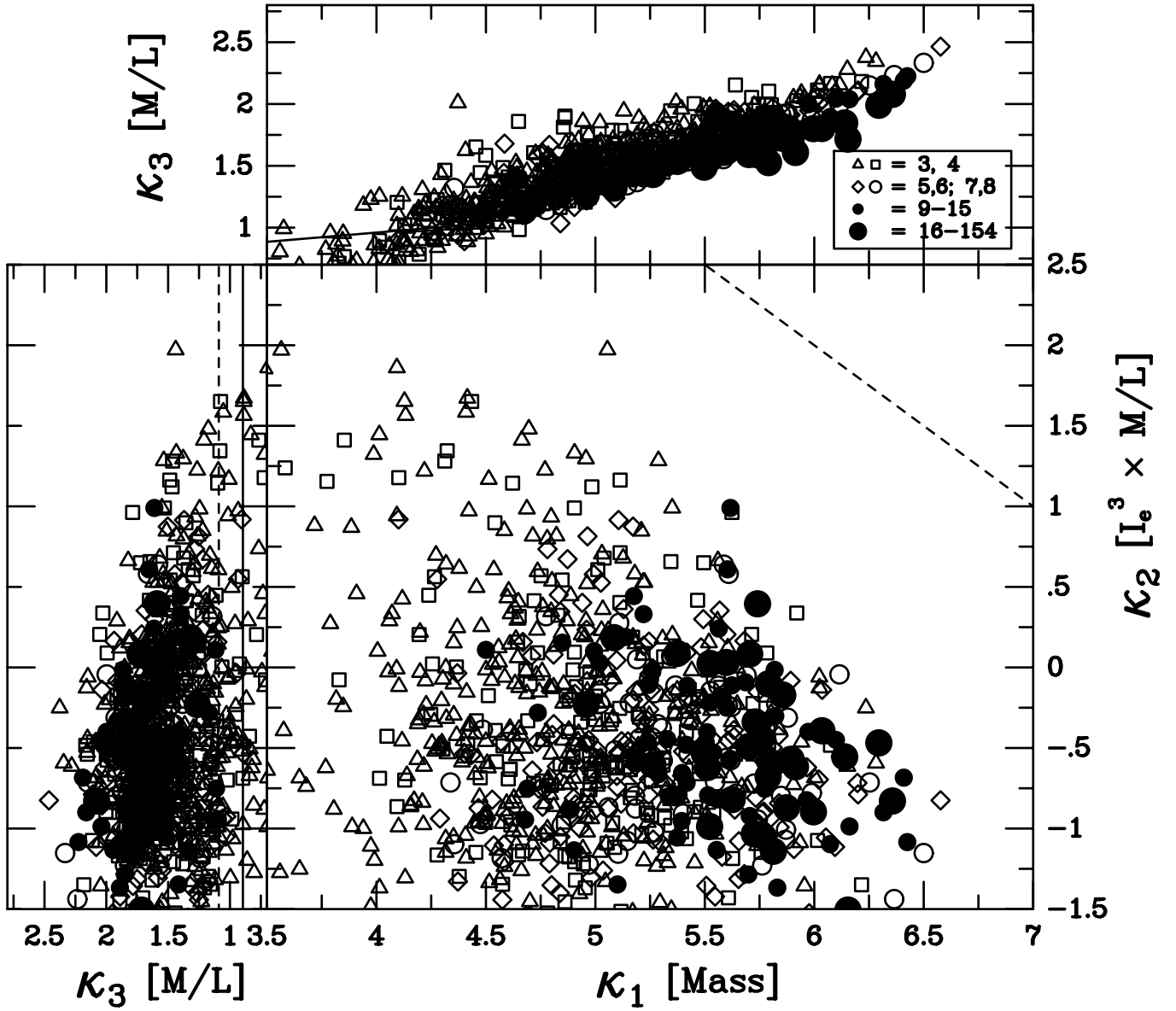
$$\text{Log } n(\text{bary}) \propto \text{Log } (\sigma^2/r_e^2) - 2.34 + S_{\text{type}}$$







CHDM₂ Simulation: Redshift-Defined Groups



CHDM₂ Simulation: Distance-Defined Groups

